BRNO UNIVERSITY OF TECHNOLOGY
VYSOKÉ UČENÍ TECHNICKÉ V BRNĚ

FACULTY OF MECHANICAL ENGINEERING
FAKULTA STROJNÍHO INŽENÝRSTVÍ

INSTITUTE OF MATERIALS SCIENCE AND ENGINEERING
ÚSTAV MATERIÁLOVÝCH VĚD A INŽENÝRSTVÍ

AB INITIO CALCULATION OF DOPING IN NI2MNGA ALLOY
AB INITIO VÝPOČTY VLIVU DOPOVÁNÍ NA SLITINU NI2MNGA

BACHELOR'S THESIS
BAKALÁŘSKÁ PRÁCE

AUTHOR
AUTOR PRÁCE
Jozef Janovec

SUPERVISOR
VEDOUCÍ PRÁCE
Ing. Martin Zelený, Ph.D.

BRNO 2018

VYSOKÉ UČENÍ TECHNICKÉ V BRNĚ
FAKULTA STROJNÍHO INŽENÝRSTVÍ

Zadání bakalářské práce

Ústav:	Ústav materiálových věd a inženýrství
Student:	**Jozef Janovec**
Studijní program:	Aplikované vědy v inženýrství
Studijní obor:	Materiálové inženýrství
Vedoucí práce:	**Ing. Martin Zelený, Ph.D.**
Akademický rok:	2017/18

Ředitel ústavu Vám v souladu se zákonem č.111/1998 o vysokých školách a se Studijním a zkušebním řádem VUT v Brně určuje následující téma bakalářské práce:

Ab initio výpočty vlivu dopování na slitinu Ni2MnGa

Stručná charakteristika problematiky úkolu:

Slitiny na bázi Ni–Mn–Ga patří mezi tzv. magnetické slitiny s tvarovou pamětí, které vykazují specifické vlastnosti a mohou najít uplatnění v široké škále oborů. Jejich výjimečnost vychází z mikrostruktury tvořené dvojčaty s vysokou pohyblivostí hranic. Tato mikrostruktura vzniká při martensitické transformaci mezi nízkoteplotní a vysokoteplotní fází, která může být ovlivněna dopováním dalšími prvky. Stabilita jednotlivých fází může být studována pomocí tzv. výpočty z prvních principů či ab initio výpočtů. Podstatou těchto metod je, že vychází pouze ze základních postulátů kvantové mechaniky a nepotřebují žádná vstupní experimentální data. Získané výsledky pak mohou sloužit k nalezení vhodného složení pro praktické aplikace či jako vstupní data pro pokročilé termodynamické modelování.

Cíle bakalářské práce:

Cílem práce je studium martensiticke transformace v dopovaných slitinách Ni–Mn–Ga pomocí ab initio výpočtů. Konkrétně bude studován vliv různých dopujících prvků na martensitická transformaci popsanou pomocí tetragonální transformační dráhy mezi austenitem a nemodulovaným martensitem. Vliv bude studován jak ve feromagnetické tak i v paramagnetickém stavu. K těmto výpočtům bude použita metoda exaktních muffin–tin orbitalů spolu s aproximací koherentního potenciálů (EMTO–CPA).

Seznam doporučené literatury:

KITTEL, C. Introduction to Solid State Physics, 6th ed. (Wiley, New York, 1986).

VITOS, L. Computational Quantum Mechanics for Materials Engineers: The EMTO Method and Applications (Springer-Verlag, London, 2007).

HECZKO, O., N. SCHEERBAUM and O. GUTFLEISCH. Nanoscale Magnetic Materials and Applications, edited by J. Liu, E. Fullerton, O. Gutfleisch, and D. Sellmyer (Springer Science & Business Media, 2009) pp. 339–439.

Termín odevzdání bakalářské práce je stanoven časovým plánem akademického roku 2017/18

V Brně, dne

L. S.

prof. Ing. Ivo Dlouhý, CSc.
ředitel ústavu

doc. Ing. Jaroslav Katolický, Ph.D.
děkan fakulty

Abstract

The subject of this work is theoretical study of Ni-Mn-Ga system, known due to the magnetic shape memory effect. Calculations were performed using the Exact Muffin-Tin Orbitals method in combination with the Coherent Potential Approximation within the Korringa-Kohn-Rostoker formalism. The total energy was calculated by Full Charge Density method. Effects of Zn or Cd dopings on total energies along the tetragonal deformation path and consequently on martensite transformation temperature T_M and Curie temperature T_C were examined. Off-stoichiometric alloys with excess of Mn at the expose of Ga were studied as well. The increase in T_M for all cases of doping in Ga sublattice and the decrease in T_M for both cases of doping in Mn sublattice were predicted. Regarding T_C, all types of doping should decrease Curie temperature with an exception of magnetic transition in the off-stoichiometric martensite.

Abstrakt

Cieľom tejto práce je teoretické štúdium systému Ni-Mn-Ga, vykazujúceho efekt magnetickej tvarovej pamäti. Pri výpočtoch bola použitá metóda Exaktných Mufiin-Tin Orbitálov v kombinácii s aproximáciou koherentného potenciálu vrámci Korringa-Kohn-Rostoker formalizmu. Totálna energia bola spočítaná pomocou metódy úplnej nábojovej hustoty. Skúmaný bol vplyv dopovania zinkom alebo kadmiom na totálne energie pozdĺž tetragonálnej deformačnej dráhy a následne na teplotu martenzitickej premeny T_M a Curieho teplotu T_C. Taktiež boli skúmané nestechiometrické zliatiny prebytkom Mn na úkor Ga. Výsledky predikujú nárast T_M po všetkých pozorovaných substitúciách v podmriežke Ga a pokles T_M po substitúciách v podmriežke Mn. Curieho teplotu znižujú všetky študované substitúcie s výnimkou zmeny magnetického usporiadania v martensite nestechiometrickej zliatiny.

Key words

Magnetic shape memory, *ab initio* calculations, Ni_2MnGa, doping, phase transformations

Kľúčové slová

Magnetická tvarová pamäť, *ab initio* výpočty, Ni_2MnGa, dopovanie, fázové transformácie

Bibliographic citation

JANOVEC, J. *Ab initio výpočty vlivu dopování na slitinu Ni_2MnGa.* Brno: Vysoké učení technické v Brně, Fakulta strojního inženýrství, 2018. 46 s. Vedoucí bakalářské práce Ing. Martin Zelený, Ph.D..

JANOVEC, J. *Ab initio calculations of doping in Ni_2MnGa alloy.* Brno: Brno university of technology, Faculty of mechanical engineering, 2018. 46 p. Supervisor Ing. Martin Zelený, Ph.D..

Declaration

I declare that I have elaborated bachelor thesis *Ab initio calculations of doping in Ni_2MnGa alloy* by myself with only help of literature and sources listed in the bibliography.

Brno, 25.5.2018

.....
Jozef Janovec

Acknowledgements

I would like to thank my supervisor, Dr. Martin Zelený, for the guidance, expert advices and ideal conditions for work on this thesis. I am also thankful to Metacentrum visual organization and Dr. Petr Šesták from CEITEC, Brno University of Technology, for allowing me to have the access to computational resources, vital for my work. My sincere gratitude goes to my family members, who were supporting me throughout my studies.

This work was supported by the Czech Science Foundation under project no. 16-00043S trough collaboration with Institute of Physics of the Czech Academy of Sciences in Prague.

Contents

Introduction

In recent decades, a lot of attention was payed to alloys showing the shape memory effect, especially to group of alloys where deformation is induced by magnetic field. This effect is called the magnetic shape memory effect and probably the most studied system exhibiting magnetically induced strain is the Ni_2MnGa alloy. Promising utilization of Ni_2MnGa in practical applications is reduced by relatively low transformation temperature of martensite, being lower than the room temperature. Therefore, a strong emphasis is given to improvement of its features, mainly transformation temperatures. Technical characteristics of Ni-Mn-Ga systems can be enhanced by change in alloy's stoichiometry or by doping with other elements.

One of the ways to study complex alloys is theoretical approach, using the *ab initio* (first-principles) calculations of electronic structure. Results obtained from theoretical calculations are generally in a very good agreement with experimental data. A numerous group of calculation methods is based on density functional theory with different approaches for solving the Kohn-Sham equations. The Exact Muffin-Tin Orbital (EMTO) method was used in this thesis in combination with the Green's-function technique. Real potentials are within EMTO approximation replaced by overlapping spherical potentials centred on every atom. Chemical disorder of substitutional alloys is treated by Coherent Potential Approximation (CPA).

The aim of this work is a description of effect of Zn and Cd doping instead of both Ga and Mn as well as a study of an off-stoichiometric alloy with excess of Mn over Ga. The calculations were focused on prediction of martensite transformation temperature and Curie temperature. Martensite was approximated by the non-modulated structure in all studied alloys. As a tool for qualitative predictions, total energy difference analysis from tetragonal deformation path was applied. This method allows us to determine only whether effect of doping on transformation temperatures is positive or negative but we cannot find its exact value. However, such information provides a useful guide for subsequent experimental research. The obtained relationships have been confirmed by the analysis of DOS for minority spin channel.

1 Thermodynamics and stability of alloys

In nature, every spontaneous process is controlled by energy minimisation of related systems and their effort to exist in the equilibrium with the surroundings. The accompanying phase transformations of any kind can be studied experimentally and described qualitatively by thermodynamics. For instance, phase transformations in solids are understood as a recast of constituents' positions aiming to get into the more stable state. These transformations are pretty much all types of structure changes, for example precipitation reactions, lattice recombination, changes in magnetic properties, etc. These structure changes may be caused by alternations of temperature, pressure, magnetic or electric fields, strain, etc. When studying phase transformations, equilibrium phase diagrams can be used as reliable tools, providing us with relations between internal properties and external conditions (mainly temperature or pressure).

In thermodynamics, a system is defined as a part of the space, separated from its surroundings by imaginary or real boundaries. The system might be composed of one or more phases, i.e. homogeneous, physically and chemically distinguishable parts of the system consisting of one or more components - either elements or chemical compounds. Phases can also be characterised by relative amounts of each component they contain. [1]

A useful overall look at both the stability of the system and the probability that a certain process happens is given by the Gibbs free energy G, called also the free enthalpy:

$$G = E_{tot} + \sum F_i + pV. \tag{1.1}$$

The sum free energies $\sum F_i$ contains terms like vibrational, rotational, translational, configurational and magnetic energy of all the components. These terms include both internal energy contribution and entropy contribution as can be seen below. The last pressure-volume dependent term is relatively small in comparison to energy terms and is often negligible. [2]

Furthermore, the total energy term E_{tot} represents the electron kinetic energy and long range electrostatic interactions between particles (ions and electrons). This energy can be obtained from the first principle calculations. [3]

As mentioned, free energies are possibly expressed in the form of $F_i = E_i - TS_i$, by applying this into the Gibbs free energy, we obtain

$$G = E_{tot} + \sum E_i - \sum TS_i + pV, \tag{1.2}$$

where S_i represents the corresponding partial entropy. The sum of all the energy contributions E_i and E_{tot}, is equal to the internal energy of a system U. In other words, the internal energy represents the sum of partial energies corresponding to both particle motion (vibrational, translational, rotational) and interactions between particles. The internal and the total energy concepts are very alike, though some important differences are present. Both are the sum of potential and kinetic contributions but internal energy is a state function of a system containing vast number of atoms and it is independent of atomic geometry. Furthermore, because of the great number of contributors, we cannot measure the exact internal energy of a specific state of the system, thus we use only changes in U. On the other hand, the total energy is an intensive property computable for a certain state and it is possible to find its value for a single atom or a molecule. [1,3]

By a simple rearrangement of terms in Eq. 1.2, the Gibbs energy can be written as

$$G = U - \sum TS_i + pV. \tag{1.3}$$

The Gibbs free energy is a quantity that gives us a relative stability of the system at a given temperature and pressure. As stated before, a system is trying to minimalize its energy to reach a stable state. Whether the transformation is likely to happen, it can be derived from the difference in Gibbs energies of both states. If it is less than zero, the change will probably carry out, being equal zero, both states are in equilibrium and if it is greater than zero, transformation will not happen spontaneously. In other words, the transformation is possible only if it results in a decrease of the Gibbs energy. In the case, when a change in the Gibbs energy is zero, but its value is not the lowest possible, the system is in metastable equilibrium. When the Gibbs energy is at the global minimum, the system is in the stable equilibrium. A negative change in the Gibbs energy is an inevitable condition for the transformation, however it is not a sufficient one since in many cases an additional energy barrier must be overcame. This barrier is explained by kinetics of phase transformations. [1]

Another thermodynamic quantity of considerable importance is the enthalpy *H*:

$$H = U + pV. \tag{1.4}$$

Under a constant pressure, the enthalpy is usually considered as an energy change in the system, being equal to the overall energy transfer from or to the environment during the reaction or transformation. As well as the internal energy, it is impossible to measure the enthalpy of a system directly hence only the change in the enthalpy is used. [4]

At zero pressure and temperature, which are assumed in this work, both temperature and pressure dependent terms are neglected in Eqs. 1.2 and 1.3. Since contributors to the $\sum E_i$ term are also temperature dependent, the change in the Gibbs free energy gets the form

$$\Delta G = \Delta U = \Delta H = \Delta E_{tot} \tag{1.5}$$

what allows us to relate the structural stability with energies obtained from the first principle calculations. [3]

The enthalpy change is also referred to as the heat of formation ΔH_f, which is defined as a change in enthalpy during the formation of a substance from its constituent elements

$$\Delta H_f = \frac{E_{product}}{N^{product}} - \sum x_i \frac{E_i}{N_i}, \tag{1.6}$$

where $E_{product}$ is the total energy of product system, subscript "*i*" represents original components (namely x_i is the stoichiometric representation of a particular component in the product), and E_i is the total energy of component in its standard state. The $N^{product}$ is a number of atoms per unit cell of the product and N_i is the number of atoms per unit cell of a corresponding element standard state. Using Eq. 1.6, one obtains the heat of formation per atom. [4,5]

2 Solid state transformations

Solid phase transformations can be categorised as diffusional and diffusionless, according to the mechanism of component reorganisation. Diffusion is a thermally activated atomic movement contributing to the decrease the Gibbs energy. Even though the diffusion is mostly connected with a decrease in concentration gradient (down-hill diffusion), in alloys exhibiting a miscibility gap, atoms are preferring the movement increasing concentration gradient (up-hill diffusion). Diffusionless transformations (so-called shear transformations) take place under conditions inconceivable for diffusion, when a co-operated movement of atoms is exhibited for shorter than interatomic distances. [1]

Another important criterion for the classification of phase transformations is the order of transformation. Discontinuities caused by temperature change such as a jump in the physical properties (crystal structure, density etc.) or temperature hysteresis and kinetics of nucleation and growth are typical indications of the first order transformations. On the other hand, the second order transformations occur at a fixed temperature, they are continuous, without a temperature hysteresis or the latent heat [6]. An example of the second order transformation is the magnetic transformation, yet, various experiments have showed the existence of a very narrow hysteresis around the temperature of magnetic transformation and there are even theories that all the transformations are of the first order. [7,8]

2.1 Martensitic transformation

Martensitic transformation is solid phase transformation, where a high temperature phase, so called austenite, transforms into a low temperature phase, so called martensite. Martensitic transformation is most commonly accompanied by a lowering of a lattice symmetry, for instance, in the case of Ni_2MnGa alloy, the cubic austenite transforms into the tetragonal martensite [9] (defined by c/a ratio, so called tetragonality, where c and a are lattice parameters). It is a diffusionless transformation since the diffusion is limited by both low temperature and high velocity of the process (it might be equal to the speed of sound in metals). As a consequence, both parent and product phases show an identical chemical composition. Martensitic transformation is one of the first order, being carried out by the mechanism of nucleation and growth. [1,10]

Considering a diffusionless character of the transformation, only a restricted coordinated movement of atoms is possible, and the interface between the austenite and martensite, called the habit plane, can be coherent or semicoherent [10]. This interface happens to be coherent in early stages of martensite formation but it changes into the semicoherent as the transformation proceeds, because of lowering the strain energy. It was observed that the growth of the habit plane is macroscopically undistorted that indicates the absence of plastic deformation during the formation of discontinuity. The motion of martensitic interface across the crystal deforms the volume of material that is associated with the formation of surface relief. [1,10,11]

The Bain model is mostly used to explain martensitic transformation in steels (Figure 2.1), where FCC→BCT transformation is described by contracting the cell of 20% in the z-direction and expanding the cell of 12% in the x- and y-directions [11]. So-called Bain strain explains how the transformation runs with the minimal atom motion. However, in the Bain model, there are not fulfilled requirements for the existence of the invariant line and the invariant plane after martensitic transformation are not fulfilled. The invariant plane and line are understood as the undeformed and unrotated crystallographic objects, common for both austenite and martensite.

The Bain strain leaves two lines undistorted, but rotated against the undeformed austenitic phase, as we can see in Figure 2.2. This problem is overcame by a rigid body rotation where one of the new phase lines overlaps one of the old phase lines and so makes it invariant (common for both new and old phase). The combination of the Bain strain and the rigid body rotation gives the observed martensitic structure, though with a wrong shape. The shape variance is solved by the formation of the macroscopic invariant plane due to an additional deformation, such as slip or twinning, associated with lowering the strain energy in the crystal (Figure 2.3). [1,10]

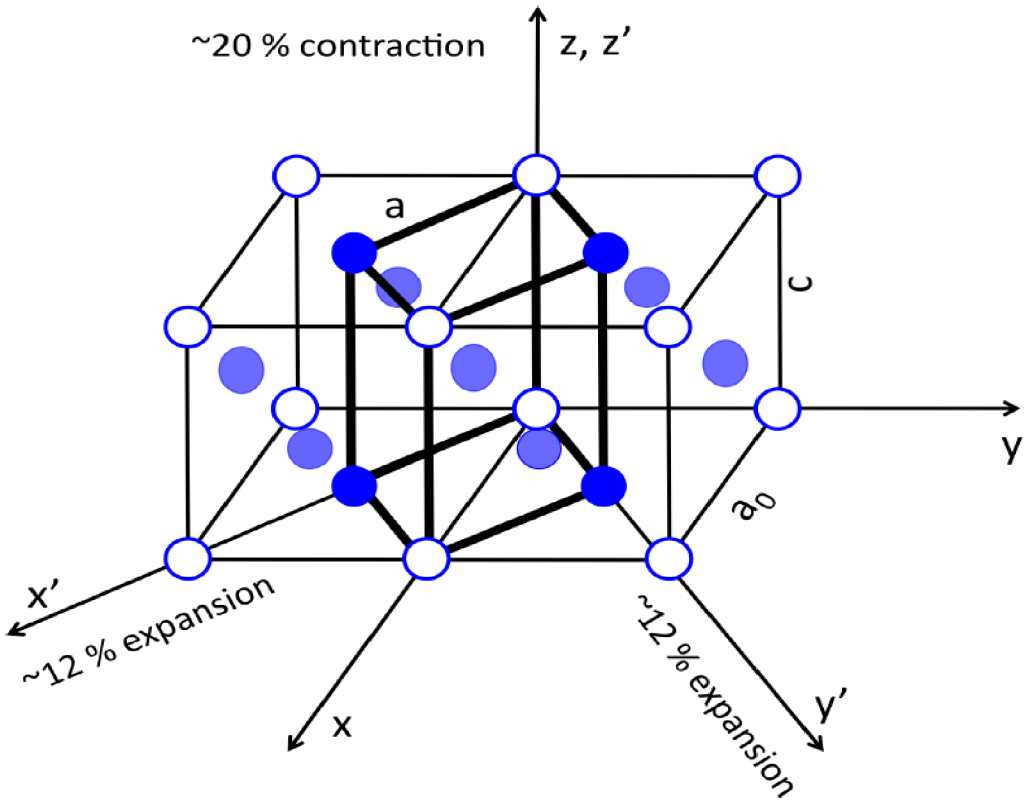

Figure 2.1 Schematic reproduction of the lattice deformation within the Bain model, a_0 represents the austenitic lattice constant, a and c are lattice constants of the new martensite phase unit cell, marked with thick lines. Adopted from [12].

By the structure formed in order to lower the elastic transformation strains, as mentioned above, we distinguish between the lens martensite, with a high density of dislocations, and the plate martensite, with a twinned structure. The transformation mechanism in the first type is performed by a shear deformation, where glide planes of slip dislocations are parallel to the habit plane and the transformation is associated with expansion that takes place normal to the habit plane. The martensite growth is provided by the formation and motion of parallel dislocations in the interface with the same Burgers vector in both phases [10]. Twinning is a preferred deformation mechanism for materials with low symmetry and large lattice parameters. In twinned martensite, the interface with austenite remains coherent. [13]

Furthermore, the martensitic transformation is mainly athermal (characterised by a rapid nucleation and growth, while the amount of transformed martensite is dependent on temperature only) or in few cases also isothermal (dependent on time). The martensitic transformation has an immense importance in various applications such as steel hardening, ceramic modification and shape memory alloys. [10]

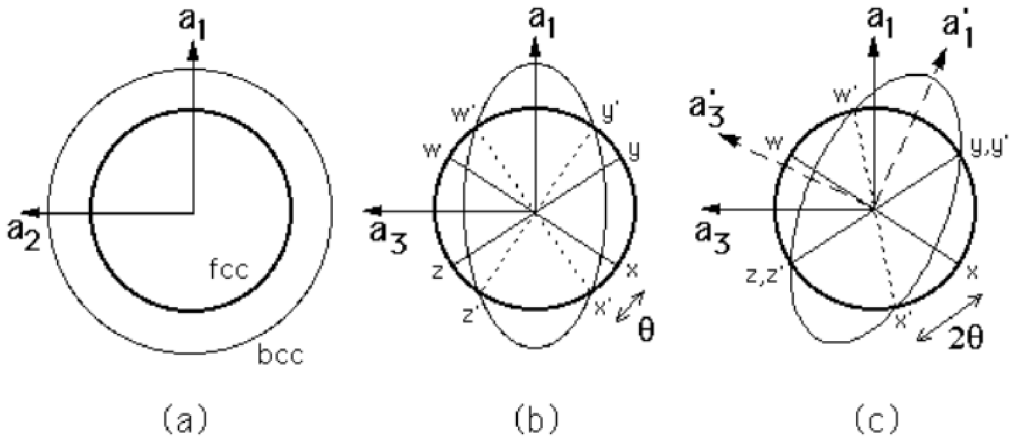

Figure 2.2 The scheme (a) represents the undistorted FCC austenite as a sphere; (b) shows the effect of the Bain strain on austenite, the ellipsoid denotes austenite deformed along the Bain path, the lines *wx* and *yz* are undeformed but rotated into new positions denoted by apostrophes; (c) combinates the Bain strain with the rigid body rotation through an angle θ that results into the existence of the invariant line *yz* = *y'z'*. Adopted from [10].

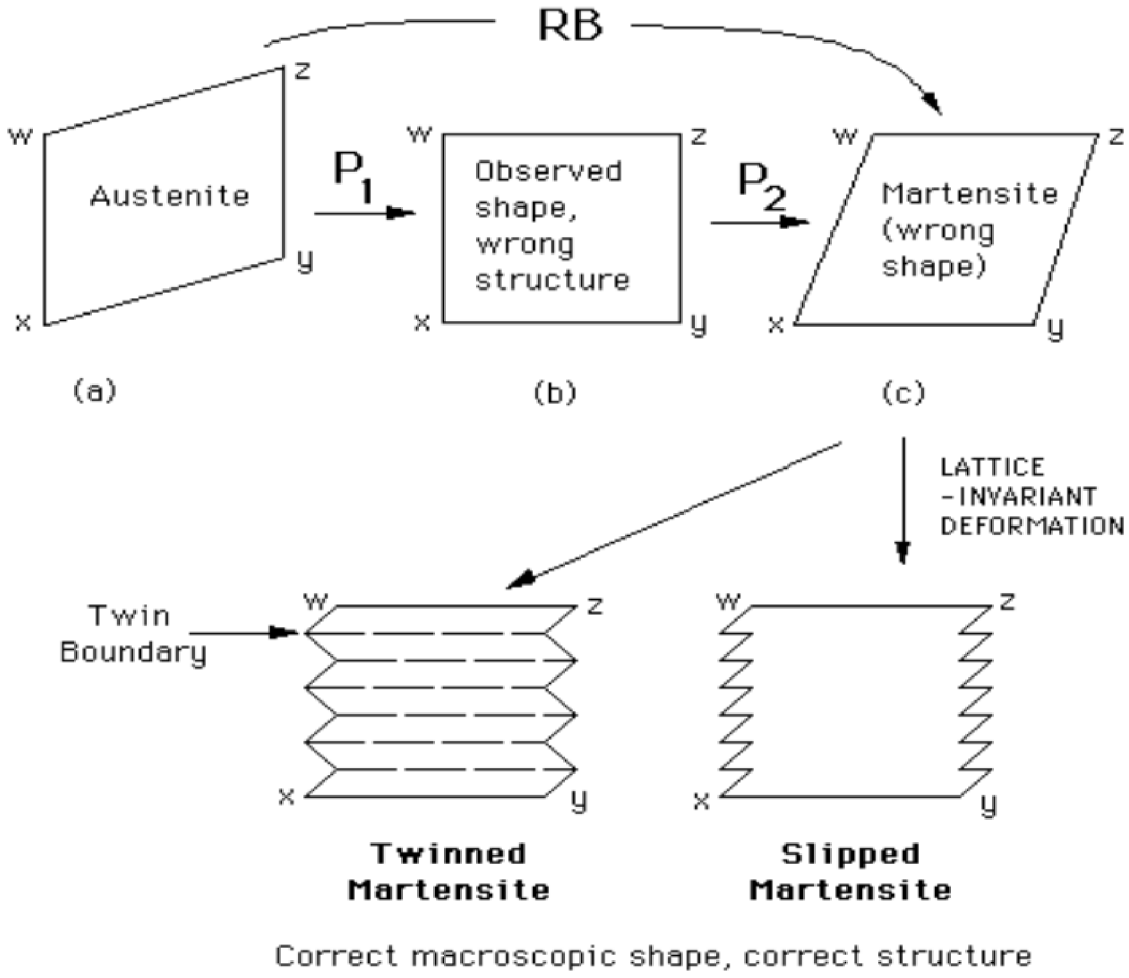

Figure 2.3 Theory of martensitic transformation. Adopted from [10].

3 Magnetic properties

Materials placed in an external magnetic field exhibit different behaviour in dependence on their composition and temperature. When an object gets into the magnetic field, all of its atoms are affected by the field, giving the object specific magnetic properties. This happens due to the fact that atoms have their own magnetic moments created by the motion of electrons that interact with the external field. As known, electrons are circulating in their orbits in the Coulomb potential of a nuclei and create their own magnetic fields since every current loop placed in an external potential creates a dipole magnetic field. Furthermore, electrons possess a built-in movement around their own axes, known as spin, also creating magnetic moment. The overall atomic magnetic moment (local moment) is determined by contribution of both orbital and spin magnetic moments of all the atom's electrons. The nuclear magnetism can be often neglected because nuclei have much greater mass than electrons (the magnetic moment is inversely proportional to the mass) [14]. Atomic magnetic moments are strongly linked to the crystal structure and thus it is unable to adjust immediately their orientation when a magnetic field is applied. [8]

The arrangement of atomic magnetic moments defines magnetic state of the material. Materials with no magnetic moment are called diamagnetics, yet by applying an external magnetic field, they generate a small magnetic field in the opposite direction to the external one. Diamagnetic materials are Zn, Cu, Bi, Au, Ag, Si, Hg or other. [14]

On the other hand, ferromagnetism is defined by the arrangement of magnetic moments of atoms in a part of the crystal in the way, that magnetic moments are heading the same direction (Figure 3.1). This behaviour results from strong crystal forces provided by a crystal field [8]. In ferromagnetic crystals, vast regions containing atoms with parallel magnetic moments are known as domains. The magnetisation of a material is defined as a vector sum of domain magnetisations. In a demagnetised state, where domains are aligned randomly, is the overall magnetisation equal to zero [15]. After an external field is applied, the domain configuration changes, domains are rebuilt in favour of well oriented domains and the crystal gets magnetised in the direction of the applied field. This phenomenon is connected with a magnetization hysteresis, caused by a continuous rearrangement of the magnetic domain structure. Ferromagnets remain magnetised even after the external field is removed. Ferromagnetic elements are Fe, Ni or Co. [14, 15]

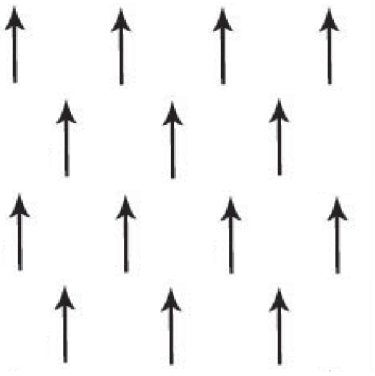

Figure 3.1 Alignment of local moments in a ferromagnetic material.

Antiferromagnetism is a special case of ferromagnetism with a zero net moment. Magnetic moments of atoms are parallel but their orientations are opposite in neighbour planes (Figure 3.2). Antiferromagnetic materials can be also described as materials with two sub-lattices being

equally magnetised in opposite directions. Some of the antiferromagnets are Mn, Cr, MnO, FeO, etc. [15]

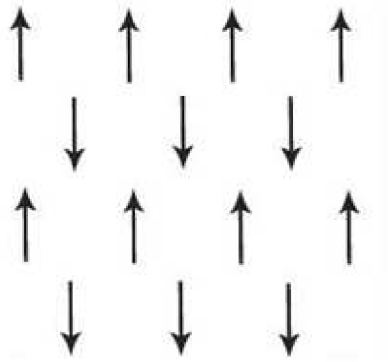

Figure 3.2 Alignment of local moments in an antiferromagnetic material

Atoms of paramagnetic materials exhibit a permanent magnetic moment but unlike in the ferromagnets, they are oriented randomly because of a thermal motion (Figure 3.3 a)). An external magnetic field causes a little arrangement of magnetic moments resulting in an occurrence of a small magnetisation in the direction of applied field [14]. The paramagnetic state can be approximated within the disordered local moment approach (DLM) represented by Figure 3.3 b), assuming the magnetically disordered system to be a pseudo-alloy of equal number of atoms with randomly distributed parallel spins with opposite orientations of their local moments [16]. The DLM approach can be used for the approximation of the paramagnetic structures in various solid state calculations. Examples of paramagnetic elements are Al, Ba, Ca, Mg, Pt etc.

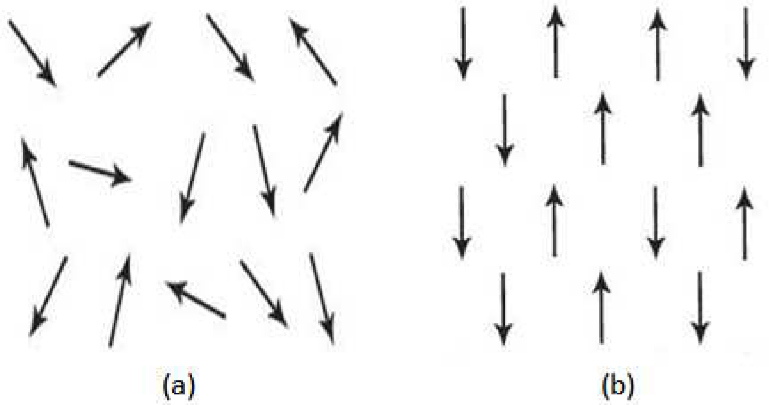

Figure 3.3 Alignment of local moments in paramagnetic materials (a) and the DLM approximation of paramagnetic materials (b).

Materials exhibiting ferromagnetism or antiferromangetism are accompanied with the magnetic anisotropy - directional dependence of magnetic properties of materials. Magnetically anisotropic materials tend to align their magnetic moments along preferable directions. Magnetization directions are hence divided into easy and hard magnetization axes. Magnetizing along the easy axis results in a rapid increase in the magnetization even in low fields. On the contrary, magnetizing in the direction perpendicular to the easy axis results in a gradual increase in the magnetization. Overall magnetization curve is a linear combination of magnetization curves of both variants and shows the hysteresis. [17]

The spontaneous magnetisation of ferromagnets and antiferromagnets is provided by an alignment of the magnetic moments and is dependent on temperature. It falls to zero at the Curie temperature [14]. In other words, the low temperature ferromagnets undergo a solid state

transformation into a high temperature paramagnetic state if the thermal motion of lattice exceeds crystal field forces.

4 Ni_2MnGa

The Ni_2MnGa alloy is a part of the alloy family, named after Friedrich Heusler, who fabricated Cu-Mn-Al alloy, the first prototype of Heusler alloys [18]. Remarkable feature of the first Heusler alloy is that none of the components is ferromagnetic while their combination shows ferromagnetism. Alloys in this group are defined as ternary intermetallic compounds characterised by a strong relationship between chemical order, composition and magnetic properties. The X-ray measurements proved that at ambient conditions, Heusler alloys crystalize in $L2_1$ structure - the FCC super lattice consisting of four sublattices [19]. If all the sublattices are filled, the alloy is called full-Heusler with the stoichiometric formula X_2YZ and the $L2_1$ lattice, however, the case with one vacant sublattice is called semi-Heusler with the composition XYZ and the $C1_b$ lattice. The letter X in generic formula stands for Co, Ni, Pd, Cu etc., Y is usually represented by Mn, Fe, Co etc., and Z is commonly Al, In, Sn, Sb, Ga etc. [12]

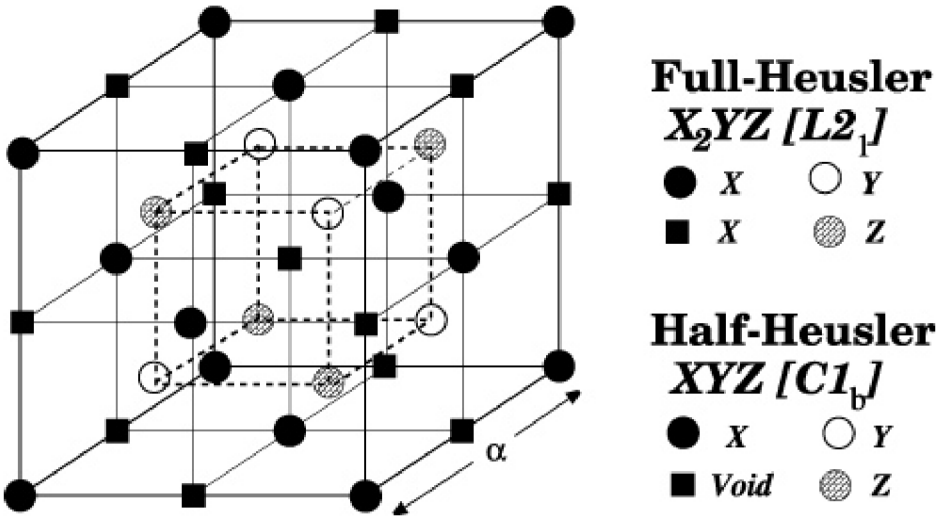

Figure 4.1 Characteristic full-Heusler superlattice $L2_1$ and half-Heusler superlattice $C1_b$. In the case of Ni_2MnGa, X sites are occupied by Ni atoms, Y and Z sites are occupied by Mn and Ga atoms respectively. [20]

The Ni_2MnGa alloy exhibits the martensitic transformation at temperatures around 202K (denoted by T_M) [21]. The structure transforms from highly symmetric high temperature cubic austenite phase into the low temperature tetragonal martensitic phase with lowered symmetry. The martensite has a twinned structure, characterised by a high mobility of twin boundaries [17]. There have been found several martensitic structures in the Ni_2MnGa - non-modulated (NM), seven-layered (14M or 7M) or five-layered (10M or 5M) [9]. The fourth theoretically predicted structure of martensite is the orthorhombic 4O structure, not proven experimentally yet. [22] Martensite structures are illustrated in Figure 4.2. The main contributor to the total magnetic moment in this alloy is manganese – the magnetic moment of the alloy is 4.17 μ_B per formula unit (f.u.) whereas the magnetic moment of Ni is less than 0.3 μ_B, and Ga exhibits neglectable magnetic moment [17]. The localized character of magnetic moments results from the exclusion of minority spin (spin down) electrons from the Mn 3*d* shell. In majority spin channel, *d* electrons of Mn join those of Ni and together form a common *d* band, while the minority spin Mn bands are pushed above the Fermi energy [23]. It leads to the ferromagnetism

due to the same spin orientation of Mn *d* electrons. The Curie temperature of the paramagnetic-ferromagnetic transformation for the stoichiometric Ni_2MnGa occurs at $T_C = 376K$ [21].

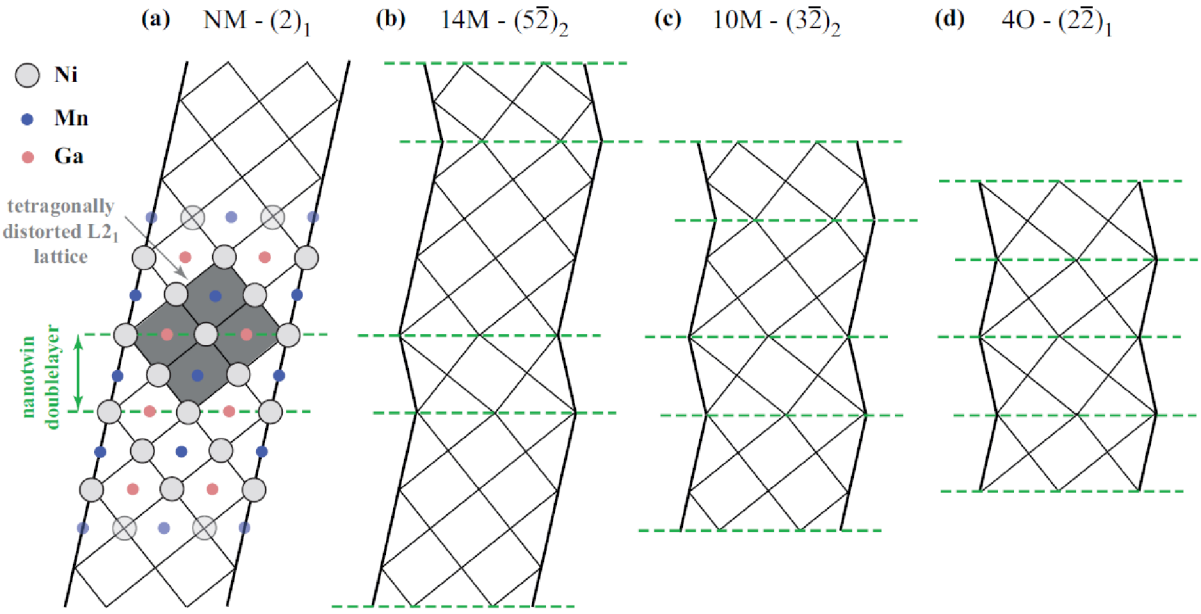

Figure 4.2 llustration of non-modulated NM martensite (a),10M (b) and 14M (c) modulated martensite, and 4O (d) martensite. The grey area in (a) represents four blocks out of eight structural blocks forming the tetragonal elementary cell. Adopted and modified from [22]

Magnetic shape memory (MSM) effect is probably the most important feature of the Ni_2MnGa alloy. For example, there was observed a magnetic field induced strain (MFIS) in 10M and 14M single crystal structures up to 6% and 10% respectively. MSM includes two effects caused by applied magnetic field – magnetically induced reorientation (MIR), done by the twin boundary motion, and magnetically induced transformation between the austenite and the martensite. Crucial for the MSM effect in Ni_2MnGa are all the existence of martensitic transformation, the formation of martensite with twinned structure and the high magnetic anisotropy. Magnetic field induces motion of the highly mobile twin boundaries, and consequently their structure reorientation. The applied field slowly rotates single crystal magnetization vector to the field direction. When the energy of the rotation surpasses the energy required for the MIR, the microstructure changes itself by nucleation and growth of twins with the favourable orientation to the field. The magnetization process is strongly dependent on the orientation of the field and shows hysteresis. MSM is applicable in various sensors, cooling systems (application of magnetocaloric effect) or, theoretically, as a source of electricity. [17]

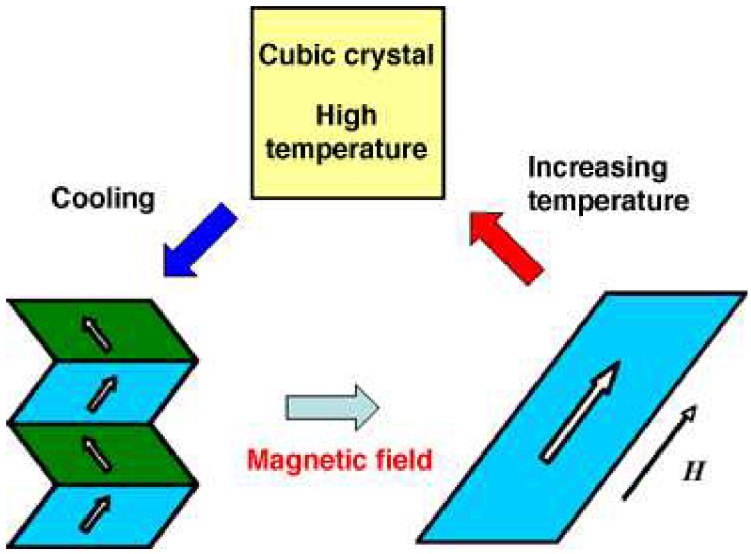

Figure 4.3 Simple scheme of MSM effect. High temperature austenite transforms into a twinned martensite on cooling. If we deform the material in the martensite phase and heat it up, it will gain the original shape of austenite. MSM effect is special because the deformation of the martensite can be caused by applied magnetic field. [24]

Investigation of the Heusler alloys gave rise to the question whether the qualitative prediction of electronic, structural and physical properties of studied compounds is possible. One of the tools for predicting the important trends in Heusler-based alloys is a dependence on the valence electron concentration per atom (*e/a*). An increase in *e/a*, as observed, is accompanied with the linear rise of T_M [25]. The valence electron concentration is related to the type of the martensitic phase structure, as well. Considering the off-stoichiometric Ni_2MnGa, for $e/a > 7.71$, NM martensite is present; in the range $e/a = 7.61\text{-}7.71$ mixtures of 10M and 14M or 14M and NM phases were observed; for $e/a < 7.61$ is dominant 10M martensite. Value of T_M in comparison to T_C is dependent on the *e/a* ratio as well – $T_M < T_C$ for $e/a < 7.67$ and $T_M > T_C$ for $e/a > 7.7$ [26]. The dependence of transformation temperatures on *e/a* for off-stoichiometric alloys is illustrated in Figure 4.4. Valence electrons are assumed to be of 3*d* and 4*s* electrons for Ni (10 electrons) and Mn (7 electrons), 4*s* and 4*p* for Ga (3 electrons). Hence, the *e/a* ratio is 7.5 for the stoichiometric alloy. The relation between *e/a* ratio and T_M might be influenced by the Fermi surface-Brillouin zone interactions. An increase in the *e/a* ratio is linked with the approach of the Fermi surface to the Brillouin zone boundary [27]. Their interaction results in formation of the pseudo-gap, visible in the density of states (DOS) diagrams, making the structure more stable what is associated with an increase of T_M. This effect is known as the Hume-Rothery stabilization. [28]

The usability of the Ni_2MnGa alloy is conditioned by T_M (it must be greater than the room temperature) and ferromagnetism of the martensitic phase. Research is therefore focused on an increase of both austenite-martensite transformation temperature T_M and Curie temperature T_C above the room temperature. One of the ways to improve characteristics of the Ni_2MnGa alloy is differentiation in the stoichiometry by increasing the concentration of one of the three components at the expose of another one. Significant improvement in physical properties can be also achieved by doping. For example, simultaneous doping by Cu and Co results in the increase of MFIS up to 12%, caused by both lowering the twinning stress and increasing both transformation temperatures above the room temperature (T_M = 330K, T_C = 393K) [29]. Furthermore, doping at the Ga-sublattice with concentration of 5 at% of Cu increases T_M up to 500 K, but decreases T_C to around 300 K. [30] In this work, we studied the influence of Zn and Cd doping at Mn or Ga sites. Zinc and Cadmium are both in the group twelve with 12 valence

electrons, considering *d* and *s* orbitals as valence. The substitution of either Zn or Cd for any atom raises the *e/a* ratio and should therefore lead to the increase in T_M. The effect of Zn was experimentally studied in the work [31]. In this work, various concentrations of Zn (from 0.75at% to 3 at%) were added into the alloy instead of Ga, which resulted in the increase in T_M to 300 K. However, the fabrication of compositionally accurate zinc-doped alloys is immensely complicated, because of Zn evaporation during alloying.

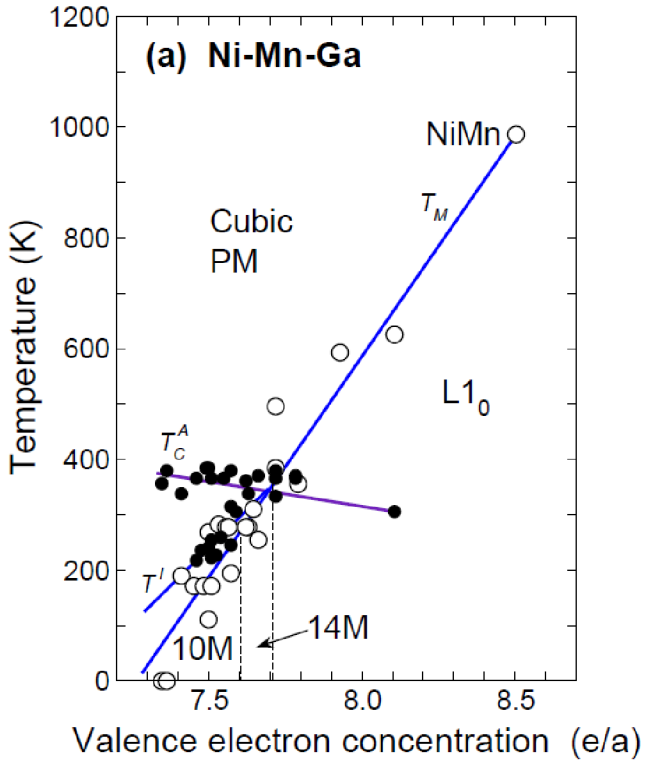

Figure 4.4 Transformation temperatures in dependence on valence electron concentration *e/a*. T_M and T' lines represent martensite and pre-martensite transformation temperatures, T_C is the Curie temperature line. Adopted and modified from [32]

Despite of a general agreement regarding the relation between *e/a* and T_M, this does not work for alloys doped by Fe to substitute Mn where T_M decrease with increasing *e/a* [5,33]. Another possibly used dependence of transformation temperature is T_M vs. *C'*, where *C'* is the tetragonal shear elastic modulus [5]. In presented work, predictions of T_M changes are based on the comparison of total energy difference between the austenite and martensite of the stoichiometric Ni_2MnGa and doped alloys [34]. Energies are obtained from *ab initio* calculations. This approach was already proven for some systems, for instance for Cu doping [30,35]. It is assumed that the bigger the energy difference is, the higher T_M. Principles of this prediction are graphically represented in Figure 4.5. The entropy term in Eq. 1.2, mostly dependent on vibration of atoms, lowers the Gibbs energy of a system more or less equally in both alloys since concentration of dopant X is considered to be low and both systems have the same crystal structure. When two alloys with just little deviations in composition are considered, their energy profiles of corresponding phases are very similar, but positions of particular profiles vary from each other. Change of total energy difference between austenite and martensite then moves the intersection of austenite and martensite profiles towards higher or lower temperature, depending on increase or decrease of total energy difference at 0 K temperature. Predicting is bases of fact that at 0 K, total energy difference is equal to the Gibbs energy change. This method allows us to make only qualitative predictions of changes in T_M, for quantitative predictions, knowledge of exact development of Gibbs energies is needed.

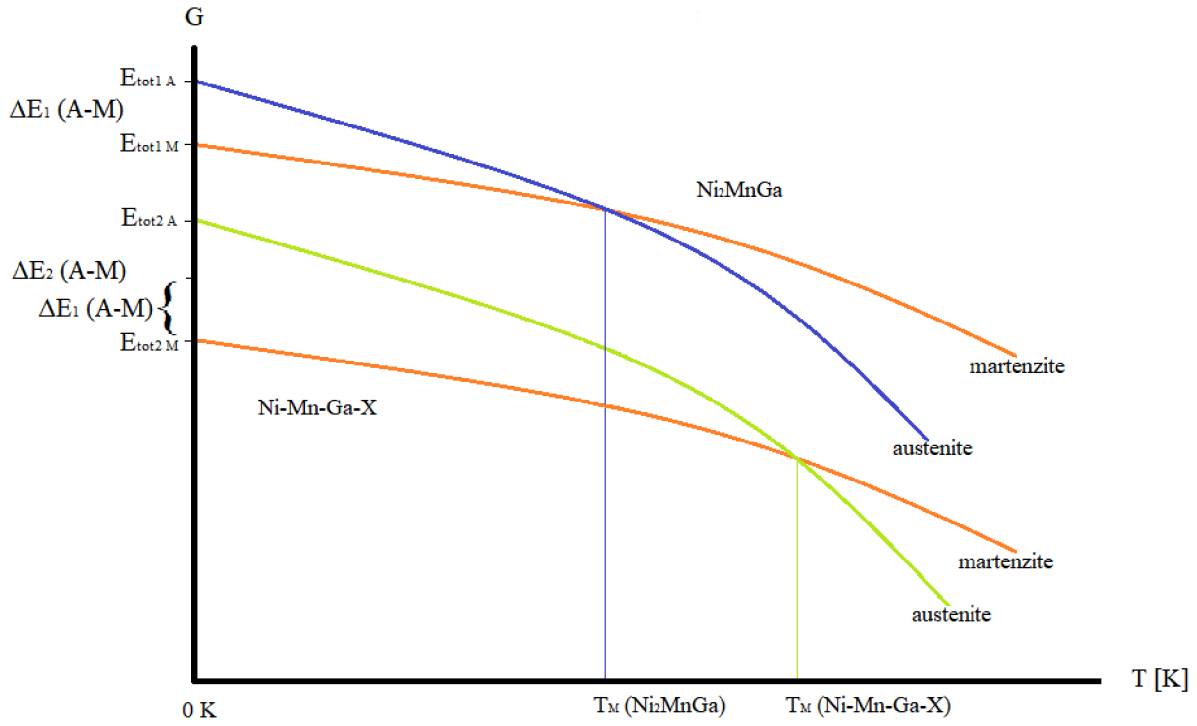

Figure 4.5 The Gibbs energy dependence on temperature. At 0 K temperature, total energy E_{tot} is equal to the Gibbs energy. $E_{tot\ A}$ represents total energy of cubic austenite and $E_{tot\ M}$ represents total energy of martensite. Martensite and austenite energy profiles are similar for nondoped and doped Ni-Mn-Ga systems with equal crystal structures.

5 Computational methods

5.1 Principles of the *ab initio* methods

A significant progress in the field of quantum physics and computational equipment has led to the formation of new, highly accurate computational techniques used for modelling and predicting properties of complex structures from their electronic structure. The cornerstone of energy calculations from the first principles is the basic problem of quantum mechanics, Schrödinger equation

$$H\Psi(r) = E\Psi(r) \tag{5.1}$$

where H is the Hamiltonian operator for energy, Ψ is the many-body wave function and E is the eigenvalue representing the total energy of the system. The wave function (eigenfunction) Ψ is a multi-component function depending in general on both positions of all the particles in the system and time. The wave function describes the state of a particle with a given energy and its square magnitude represents the probability of finding the particle in a given location. When studying a crystal structure, the solution of the Schrödinger equation is an energy of electron moving in an external nuclei potential field. [3]

To analyse a quantum system, we must find the Hamiltonian – the total energy operator, consisting of kinetic and potential energies

$$H = -\sum_{i=1}^{N_e} \frac{\hbar^2 \nabla_i^2}{2m} - \sum_{i}^{N_e}\sum_{j}^{N_n} \frac{e^2 Z_j}{|\vec{r_i} - \vec{R_j}|} + \sum_{j<i}^{N_n} \frac{e^2 Z_i Z_j}{|\vec{R_j} - \vec{R_i}|} + \sum_{j<i}^{N_e} \frac{e^2}{|\vec{r_j} - \vec{r_i}|}. \tag{5.2}$$

The first term is the kinetic energy operator, where N_e is the number of electrons, $\hbar$ is the reduced Planck constant, ∇ is the Laplacean operator and m stands for the mass of an electron.

Other three terms are contributions to operator for potential energy, N_e is the number of nuclei, r and R are positions of electrons and nuclei respectively, e is the elementary charge and Z is the protone number. The first sum represents kinetic energy of moving electrons, other sums stand for potential energy with contributions from all electron-nuclei interactions, nuclei-nuclei interactions and electron-electron interactions respectively. The presented notation is allready sympified by Borh-Oppenheimer approximation, reflecting that kinetic energy of nuclei is neglected, because electrons are much lighter than nuclei. Even after this approximation, especially the electron-electron term makes calculations for bigger systems computationally intensive and further symplifications are innevitable. [3,36]

Another approximation, made in order to ease an extensive problem is the Hartree-Fock approximation. The simplification is obtained by considering non-interacting electrons described by the multi-electron wave function expressed by the Slater determinant that satisfies both anti-symmetry and Pauli principle by changing sign on exchange of two electrons. Energy difference between exact and Hartree-Fock solution is partly fixed by including the exchange energy, describing the interaction between electrons with parallel spins. Later approximation is given by the density functional theory (DFT) where the difference from the Hartree-Fock method is the inclusion of the exchange-correlation potential. [3,37]

Nowadays, DFT is probably the most commonly used approach to *ab initio* calculations. The main asset of DFT is a replacement of the *N*-electron wave by the electronic density functional, which is only a function of three variables (space dimensions) [36]. The basic assumptions of DFT are Hohenberg-Kohn theorems, first of which says, that the external potential and the total energy are unique functionals of the electron density. The ground state electron density $n_0(r)$ can be calculated from the corresponding many-body ground state wave function $\Psi_0(r_1, r_2, \dots, r_N)$ and both functions carry exactly the same information [38]. The ground state electron density is calculated as the sum of square magnitudes of single electron wave functions bellow the Fermi energy

$$n_0(r) = \sum_{\varepsilon_i \leq E_F} |\Psi_i(r)|^2. \tag{5.3}$$

The second Hohenberg-Kohn theorem states, that the ground state energy (the lowest possible energy of a system) is proportional to the ground state density. [3]

In DFT, non-interacting electrons are considered, moving in an effective potential instead of many-body interacting electrons in the potential of static nuclei. The effective potential is a function of the total charge density originating from effects of all electrons and nuclei. Electron density and the total energy of the system are obtainable from solving the set of single-electron equations. This approach is known as the Kohn-Sham scheme [39] in which the one electron Schrödinger equations $\Psi_i(r)$, also called the Kohn-Sham equations (Eq. 5.4), are solved.

$$\left[-\frac{\hbar^2 \nabla_i^2}{2m} + v[n(r)]\right] \Psi_i(r) = \varepsilon_i \, \Psi_i(r) \tag{5.4}$$

In Kohn-Sham equations, the effective potential $v[n(r)]$ consists of the nuclei external potential, the Hartree potential arising from the electron-electron interactions and the exchange-correlation potential including mutual repulsion of electrons due to the Pauli exchange interaction. The difficulty of the initial problem is hidden in the exchange-correlation part of

the potential and the accuracy of DFT is influenced only by approximate functionals describing the exchange and correlation energies. [3,36]

The total energy of a system can be written as

$$E_{tot} = \sum_i \varepsilon_i - \int n(r) V_{xc}[n(r)] - E_H[n] + E_{xc}[n] \tag{5.5}$$

where the first term represents eigenvalues of the Kohn-Sham equation (Eq. 5.4) for every electron, next term contains the exchange-correlation potential $V_{xc}[n(r)]$ and remaining terms are the Hartree energy functional $E_H[n]$ and the exchange-correlation energy functional $E_{xc}[n]$. [36,40]

The Kohn-Sham equations are solved in a self-consistent way, meaning that they are calculated for changing set of initial inputs until the convergence is reached. In practice, we start with an initial guess for the electron density from the set of basis wave functions, then compute corresponding potentials and solve the Kohn-Sham equations. This process is then repeated for different electron densities guesses until the convergence is achieved. Finally, the total energy is calculated for the converged $n(r)$. [36]

5.2 The EMTO method

One of the methods used for solving the Kohn-Sham equations is the muffin-tin approximation. Within this approximation, the effective potential is represented by a non-overlapping spherically symetric potential spheres around the nuclei and a constant potential in the intersticial region. The potential field within this approach is not in a very good agreement with the reallity. An important improvement was made by Andersen and co-workers by developing the Exact Muffin-Tin Orbitals (EMTO) theory [41] based on an exact solution of single electron equations for the optimized overlapping muffin-tin potential. The overlapping spherical potentials provide much more reallistic approximation. EMTO is a cellular method, meaning that the single-electron Schrödinger equations are solved for units defined for every lattice in a way they give a proper description of the local surroundings. The potential is approximated by the optimized overlapping muffin-tin potential spheres. Within the EMTO method, the Korringa-Kohn-Rostoker method (KKR) is used to solve Kohn-Sham equations [42]. Although the DFT was in the previous section introduced using the wave function formalism, the KKR works with the Green function formalism. The advantage of this approach is that we only need to calculate a derivative the Green function to get the electron density instead of solving the wave function problem. The Green function formalism is more computationally demanding, but it is suitable for studying disordered systems such as impurities, for instance within the Coherent Potential Approximation (CPA). [43]

The most powerful approximation to treat systems with substitutional disorder is considered to be CPA, where an alloy is replaced by an ordered effective medium described by the site-independent coherent potential. The impurity problem is then treated within the single-site approximation (Figure 6.1). Effect of the local environment is neglected, thus the local potential around a certain alloy component is independent on its position in the crystal. There exist many applications for this approximation. We can calculate lattice parameters, bulk modulus, enthalpy of formation etc. However, CPA fails in some applications, for example, it cannot take into account the effect of short range order, and systems with large size difference between the alloy components are difficult to describe, because local lattice relaxations are not considered

in the CPA approximation. Fortunately, this is not a problem in Ni_2MnGa [44]. The CPA can also be applied to paramagnetic systems within DLM approximation. [45]

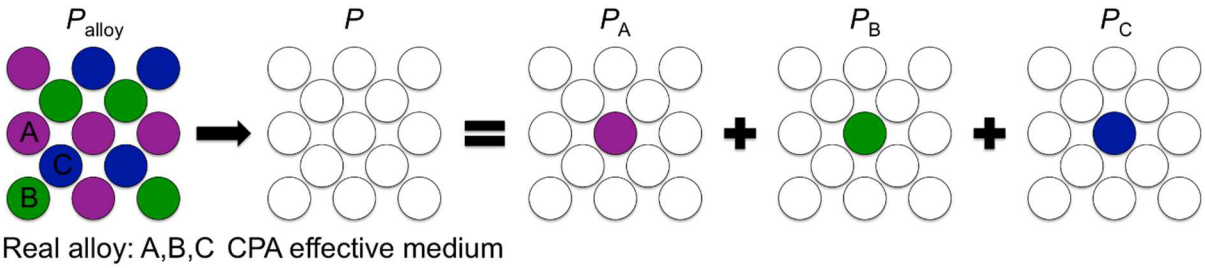

Figure 6.1 Within the CPA approximation an alloy is replaced by an effective medium, the parameters of which are determined self-consistently. The local potentials around a certain type of atom in the alloy are the same everywhere in the alloy. Thus, the real Green's function of the alloy is approximated by a coherent Green's function, calculated using an electronic structure method (EMTO). [46]

For purpose of this work, the EMTO-CPA calculations were used, namely its emto-5.7 package version. This package consists of five programs – *bmdl, kstr, shape, kgrn* and *kfcd*. The *bmld* package is responsible for the Madelung potential calculation. An electron feels the attractive potential from nuclei and repulsive potential from other electrons. Both the potentials have long range effect, and therefore they affect particles outside the unit cell as well. This outer effect is called the Madelung potential. [47,48]

The second package *kstr* provides calculations of energy dependent slope matrix in real space. Within the EMTO method, the orbitals are constructed using different wave functions inside the muffin-tin potential spheres and in the interstitial regions. Wave functions inside the interstitial regions are referred to as the screened spherical waves, being dependent on elements of the slope matrix, calculated by *kstr.* [47,48]

The next package is called *shape* and its function is a computation of the shape function, which transforms any integral over the Wigner-Seitz cell into an integral over a sphere surrounding the unit cell. [36,47]

The *kgrn* package solves the Kohn-Sham equations self-consistently using the EMTO-CPA formalism. The *kfcd* takes the converged total electron density created by *kgrn*, and evaluates the DFT total energy functional in order to produce the ground state total energy of the system [48]. This total energy is obtained by implementing the Full Charge Density (FCD) technique that uses the total charge density to compute the total energy from the Eq. 5.5. The FCD technique assumes the knowledge the spherically symmetric part of the potential only, but uses the non-spherical full charge density. In order to calculate the space integrals in the Eq. 5.5 we use the shape function technique [36].

5.3 Calculation set up

The *ab-initio* calculations were preformed using the EMTO-CPA method in combination with the KKR formalism and the Green function approach. The total energy was calculated by the FCD technique. The exchange-correlation term was described within the Perdew-Burke-Ernzerhof (PBE) generalised gradient approximation [49], and the scalar-relativistic and soft-core approximations were used. The effect of the charge misfit on the spherical potential is taken into account using the screened impurity model in [50] and [51]. Described combination of methods is suitable for an accurate characterization of chemically disordered structures caused by doping and for the determination of the total energy with respect to anisotropic lattice distortions such as the tetragonal deformation. [35]

As for the EMTO basis set, the *s*, *p*, *d* and *f* orbitals were included and as the valence orbitals were considered Ni $3d^8\ 4s^2$, Mn $3d^5\ 4s^2$, Ga $3d^{10}\ 4s^2\ 4p^1$, Zn $3d^{10}\ 4s^2$ and Cd $4d^{10}\ 5s^2$. In order to get a better agreement with experiment for non-modulated martensitic structure, the muffin-tin potential on the Ni sublattice was optimized by choosing the atomic radius $R_{ws}^{\mathrm{Ni}} = 1.10R_{ws}$ and the overlapping potential sphere radius $R_{mt}^{\mathrm{Ni}} = 0.95R_{ws}$, where R_{ws} is the average Wigner-Seitz radius [52,53]. The Green's function was calculated for 32 complex energy points distributed exponentially on a semi-circular contour. The Brillouin zone was defined on a 13 x 13 x 13 uniform *k*-point mesh without ant smearing technique [35].

6 Results

As mentioned above, aim of the presented work is the study of effects of Zn, Cd and Mn doping on Ni_2MnGa alloy in both ferromagnetic (FM) and paramagnetic (PM) states. From the development of total energy along the tetragonal deformation path, we can qualitatively estimate and compare influence of doping on transformation temperature T_M. As previous works declare, changes in T_M are related to the austenite – martensite energy difference in the FM state [30,34,35], since the ground state structure is the ferromagnetic martensite. Even though the tetragonal non-modulated martensite is not a ground structure of the stoichiometric alloy, it serves as an appropriate and precise model as there are small energy differences between the NM and modulated structures [22]. On the other hand, the energy difference between the FM and PM states can be used as a tool for the prediction of Curie temperature T_C [54,55]. The disorder of magnetic moments in PM state was simulated by the DLM approximation (Figure 3.3 b) where Mn atoms with the opposite orientation of magnetic moments are randomly distributed in the manganese sublattice.

Calculations were carried out for 2.5 at% and 5 at% of Zn or Cd, substituting atoms in both Ga and Mn sublattices and for 3.125 at% and 6.25 at% of Mn in Ga sublattice, where substituted Mn atoms exhibit opposite orientation of magnetic moments than in Mn sublattice [56]. Structural stability of studied structures was examined by heat of formation and the DOS analysis of electronic structure were carried out for FM states, correlating effects of dopants and stability with the electronic structure.

6.1 The equilibrium volume and magnetic properties

The first step in the investigation of the tetragonal deformation path of different systems is to find its equilibrium volume, in order to calculate correct total energies. Equilibrium volumes are determined by the lowest energy. Calculations of tetragonal deformation paths were performed for the equilibrium volume V_{0A} of the austenite primitive cell because the difference between the austenite and NM martensite equilibrium volumes is minimal, especially for low concentrations of dopants and therefore the energies along the deformation path are sufficiently accurate when using the austenite equilibrium volume for every *c/a*. [35]

Table 1 Calculated austenite primitive cell equilibrium volume V_{0A} in both FM and PM states and heats of formation for selected alloys. Results for Ni_2MnGa are compared with other theoretical (obtained by PAW method) and also experimental data.

Alloy	V_{0A} [Å^3/f.u.]	ΔH_f^A [eV/f.u.]	Alloy	V_{0A} [Å^3/f.u.]
FM $Ni_{50}Mn_{25}Ga_{25}$ (this work)	49.105	-0.3052		
PAW method	49.081 [57]	-0.2993 [58]	PM $Ni_{50}Mn_{25}Ga_{25}$	49.176
Experimental data [59]	49.284	-0.3089 ± 0.0404		
FM $Ni_{50}Mn_{25}Ga_{20}Zn_5$	48.969	-0.2855	PM $Ni_{50}Mn_{25}Ga_{20}Zn_5$	49.070
FM $Ni_{50}Mn_{20}Ga_{25}Zn_5$	49.101	-0.3118	PM $Ni_{50}Mn_{20}Ga_{25}Zn_5$	49.166
FM $Ni_{50}Mn_{25}Ga_{20}Cd_5$	50.364	-0.2262	PM $Ni_{50}Mn_{25}Ga_{20}Cd_5$	50.470
FM $Ni_{50}Mn_{20}Ga_{25}Cd_5$	50.444	-0.2562	PM $Ni_{50}Mn_{20}Ga_{25}Cd_5$	50.505
FM $Ni_{50}Mn_{31.25}Ga_{18.75}$	48.998	-0.2433	PM $Ni_{50}Mn_{31.25}Ga_{18.75}$	49.177

The results of calculations focused on finding the equilibrium volume in the FM state are shown in Figure 6.1 a). Cadmium increases V_{0A} in both Mn and Ga sublattices the most, the equilibrium volume is slightly greater when Cd substitutes Mn (Cd → Mn). These effects are easily trackable as results of larger atomic size of Cd. On the other hand, the influence of Zn is opposite to that of Cd. Zn → Ga substitution decreases V_{0A} and the Zn → Mn substitution does not have any significant effect on V_{0A}. Effect of Mn in Ga sublattice is alike to the effect of Zn being in the same sites. The results for the PM state are presented in the Figure 6.1 b) and show the same trends as observed in the FM state. Equilibrium volumes for some dopant concentrations are listed in Table 1 for both FM and PM states.

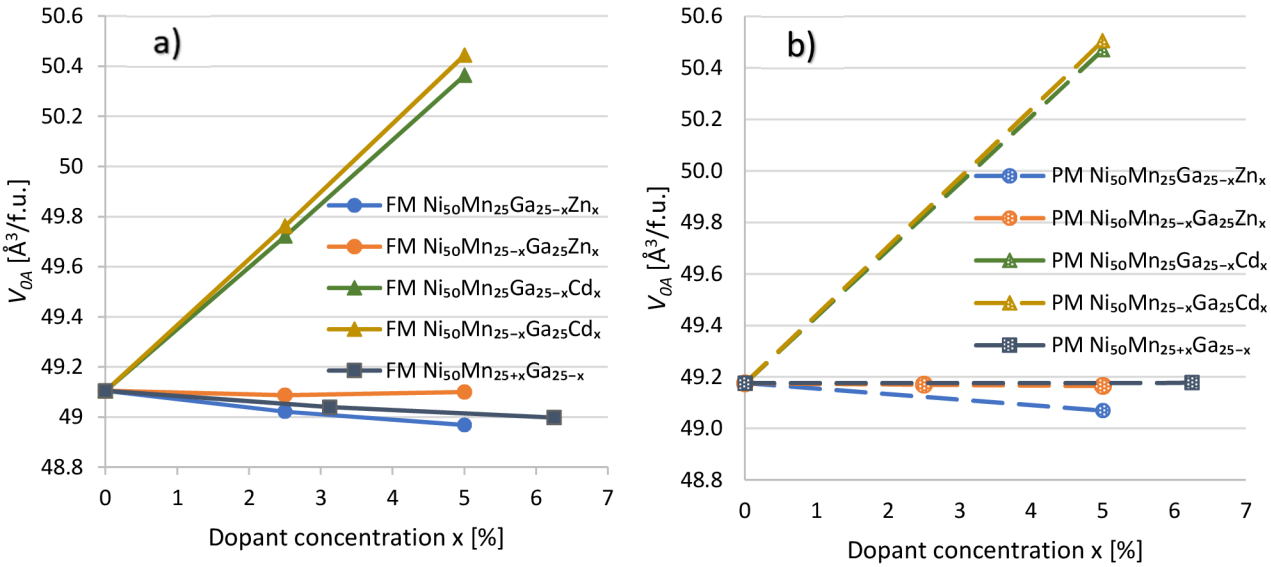

Figure 6.1 Effects of dopants on equilibrium volume of primitive cell of the austenite in a) FM state and b) PM state for different concentrations. Point x = 0 represents V_{0A} of the FM stoichiometric Ni_2MnGa.

Considering magnetism of alloys, constituents in their standard states are ferromagnetic nickel, antiferromagnetic manganese and diamagnetic gallium. Responsible for ferromagnetic nature of Ni_2MnGa is therefore mainly manganese and partly nickel. Substituents considered in this work are from the twelfth group (Zn and Cd) and hence they are both diamagnetic. This means doping by Zn or Cd should not have any major impact on magnetic properties of the alloy when substituting Ga atoms and should decrease the alloy total magnetic moment when substituting Mn atoms. Local magnetic moments of Ni and Mn as well as total magnetic moments per unit cell are listed in Table 2, all the other constituents present in individual alloys have magnetic moments lower than 0.1 μ_B. It can be seen that in all cases of doping at Mn sites, total magnetic moment falls down and doping at Ga sites have almost no effect on magnetic moment.

6.2 Thermodynamic stability

In aim to prove thermodynamic stability of studied alloys, calculations were carried out to obtain their standard heats of formation. The concept was based on the assumption of theoretical reaction of

$$2Ni + (1-x)Mn + (1-y)Ga + (x+y)X \rightarrow Ni_2Mn_{1-x}Ga_{1-y}X_{x+y}. \qquad (6.1)$$

The concentrations of reactants within this equation vary from alloy to alloy, depending on the amount of dopant X (X = Zn/Cd) and on the sublattice element that is replaced. For the case of an increase of Mn component at the expense of Ga, the theoretical reaction can be written as

$$2Ni + (1+z)Mn + (1-z)Ga \rightarrow Ni_2Mn_{1+z}Ga_{1-z}. \quad (6.2)$$

The heat of formation is then obtained by implementing the Eq. 1.6, where the energies E_i represent calculated total energies of constituent elements in their pure crystalline forms. For this purpose, we assumed the ferromagnetic FCC nickel, antiferromagnetic manganese approximated by FCC lattice, diamagnetic FCC gallium and diamagnetic HCP zinc and cadmium. Heats of formation were calculated for cubic austenite.

Heats of formation for some alloys are presented in Table 1. All heats of formation are negative, meaning that components are more stable in alloys than in separated standard forms. In other words, it proves that studied alloys are possible to fabricate. The heats of formation were calculated for cubic austenite.

6.3 Zn, Cd and Mn doping effect on tetragonal deformation

The results of calculations of the total energy development along the tetragonal deformation path in the FM state is presented for both doping by Zn and Cd separately and then compared to each other. The total energy is a function of tetragonality along the tetragonal deformation path. For better visualisation, deformation paths are plotted with respect to the austenite energy since absolute total energies of different alloys significantly vary. In all figures, the austenite total energy is set to be equal zero and all plotted energy points are obtained as a subtraction of the austenite total energy from the absolute total energies along the deformation path.

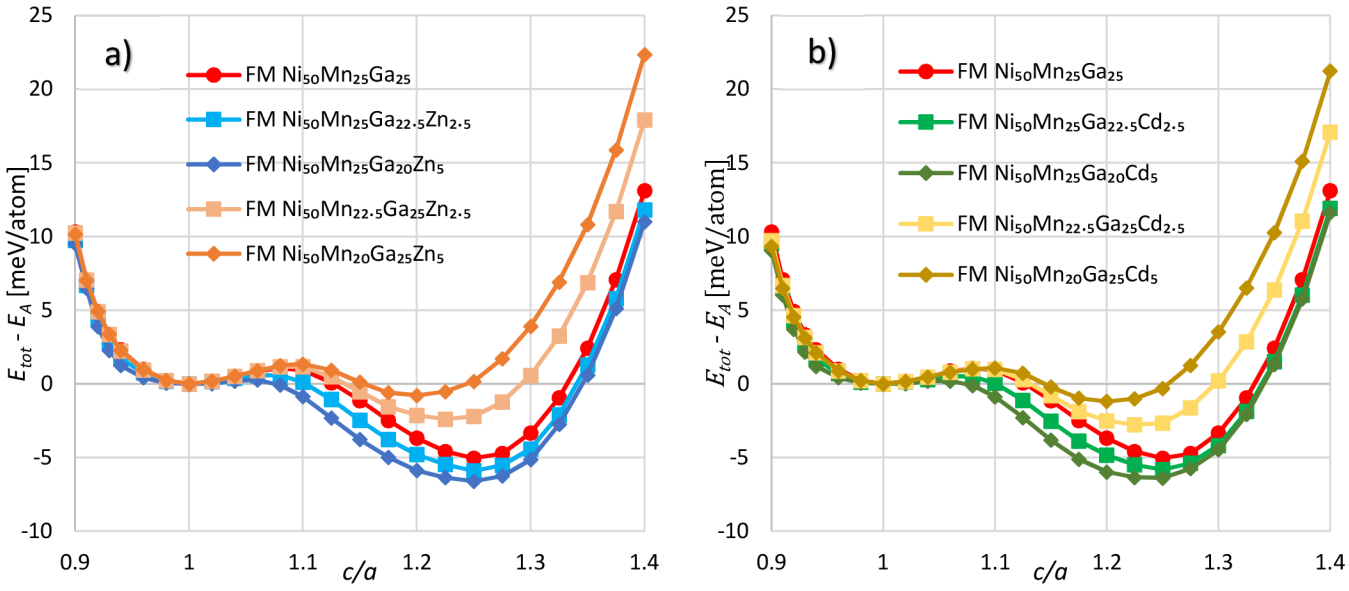

Figure 6.2 Difference of calculated total energies and austenite total energy dependence on *c/a* for case of a) Zn → Mn and Zn → Ga and b) Cd → Mn and Cd → Ga substitution for various concentrations.

The results obtained for stoichiometric Ni_2MnGa in both FM and PM states (highlighted in red in all plots), are taken as a reference values for all modified alloys. In all figures, Ni_2MnGa is represented by red colour. The tetragonal deformation path of the undoped alloy shows two energy minima and a barrier between them (Figures 6.2-6.3). The minimum occurring at $c/a = 1$ represents the $L2_1$ cubic austenite. The second minimum occurs at $c/a \approx 1.25$ and

represents the NM tetragonal martensite. Experimentally observed tetragonality of NM martensite is equal to $(c/a)_{NM} \approx 1.17 - 1.23$ [29], that is little smaller than calculated value, but all *ab initio* methods underestimate tetragonality [35]. Energy at $c/a = 1$ in all energy profiles of doped alloys belongs to the cubic austenite and energy minima at higher c/a belongs to the NM martensite. The energy barrier at $c/a \approx 1.09$ indicate that austenite is stable with respect to the tetragonal deformation. The existence of the barrier may prevent austenite from transforming into the NM martensite, hence we suggest that the ground state structure is different from the NM martensite, e.g. 10M or 14M martensite. Recent theoretical results show that the transformation path of this alloy to 10M martensite does not exhibit any energy barrier [60], which corresponds to experimentally observed 10M martensite near 0K [32]. If there is no energy barrier on the tetragonal deformation path, the austenite is unstable with respect to such deformation and the cubic structure can freely transform into the NM martensite at 0 K. The energy barrier is the reason why the ground state structure of Ni_2MnGa is different.

The results for Zn doping are shown in Figure 6.2 a). It is clearly visible that Zn → Mn substitution leads to both destabilization of NM martensite (the martensite energy minimum is at higher ΔE than that in the undoped alloy) and reduction of its tetragonality $(c/a)_{NM}$. Also, the energy maximum moves towards higher c/a and energy difference that may indicate an increase in stability of the austenite phase ($c/a = 1$). On the contrary, Zn → Ga substitution has an opposite effect, total energy of the NM martensite is lower for modified alloys and energy barrier between austenite and martensite gets smaller. Both of these factors are in favour of prediction of more stable NM martensite. In the latter substitution, the tetragonality changes only slightly. Tetragonalities for different concentrations are displayed in Table 2.

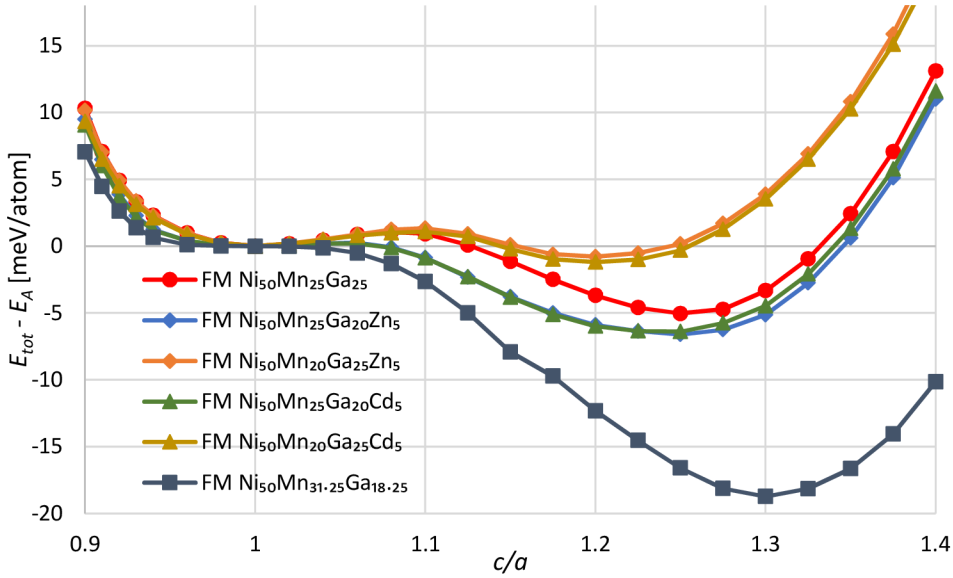

Figure 6.3 Comparison of total energy difference versus c/a for 5 at% of Zn or Cd substitutions in both Mn and Ga sublattices and 6.25 at% of Mn substitution in Ga sublattice.

The results for doping with Cd are shown in the Figure 6.2 b). Total energy profiles above the profile of the stoichiometric Ni_2MnGa characterise Cd → Mn substitution. Tendencies are the same as for the Zn → Mn substitution, the martensitic phase is less stable comparing to the undoped alloy, tetragonality of the martensite decreases. The energy barrier between austenite and martensite for the Cd → Mn doping is almost unchanged, compared to the Zn → Mn doping. The substitution of Cd atoms into the Ga sublattice has also similar effect as reported for the Zn → Ga doping. The only difference is that Cd doping gently lowers the tetragonality

of martensite. The comparison of zinc and cadmium effects is plotted in Figure 6.3, where the results for 5 at% of dopants are shown, since they have stronger effect. In Figure 6.3 energies along the tetragonal path for Mn → Ga substitution are also plotted. It shows much deeper minimum of the NM martensite comparing to Zn or Cd doping. It is observable that Zn and Cd doping have almost the same effect on Ni-Mn-Ga tetragonal path.

Table 2 The local magnetic moments in μ_B per atom of Mn, Ni and total magnetic moment in μ_B per formula unit for austenite and nonmodulated martensite and tetragonality of martensite for different compositions. All values were calculated for the FM state.

	AUSTENITE			MARTENSITE			
Alloy	Mn [μ_B]	Ni [μ_B]	μ_{tot} [μ_B/f.u.]	Mn [μ_B]	Ni [μ_B]	μ_{tot} [μ_B/f.u.]	$(c/a)_{NM}$
$Ni_{50}Mn_{25}Ga_{25}$	3.52	0.33	4.11	3.43	0.38	4.11	1.252
$Ni_{50}Mn_{25}Ga_{20}Zn_5$	3.51	0.34	4.12	3.43	0.38	4.11	1.243
$Ni_{50}Mn_{20}Ga_{25}Zn_5$	3.52	0.29	3.69	3.48	0.37	3.81	1.202
$Ni_{50}Mn_{25}Ga_{20}Cd_5$	3.57	0.33	4.17	3.49	0.38	4.18	1.237
$Ni_{50}Mn_{20}Ga_{25}Cd_5$	3.57	0.26	3.31	3.53	0.34	3.44	1.204
$Ni_{50}Mn_{31.25}Ga_{18.75}$	3.50	0.26	3.70	3.39	0.27	3.10	1.302

6.4 Prediction of the austenite-martensite transformation temperature

The main goal of doping in Ni-Mn-Ga is to increase the martensite transformation temperature as well as the Curie temperature. As mentioned in the section 4, trends and changes of T_M can be predicted from the knowledge of tetragonal deformation paths. Whether T_M increases or decreases, it is predicted by comparing austenite and martensite total energy difference of studied system with a reference system (in our case the reference alloy is stoichiometric Ni_2MnGa). If the difference for doped system is greater than that for referential one, the growth of T_M can be predicted. Similarly, the smaller energy difference corresponds to the decrease in T_M. The results presented in the previous section show a deepening of martensite energy minimum when the Ga-sublattice is doped by whichever dopant. Conversely, substitution of Mn atoms resulted in the destabilization of martensite. Described effects are summarised in Figure 6.4 and in Table 3.

In Figure 6.4, the y-axis represents energy difference between austenite and non-modulated martensite in meV/atom and the x-axis shows concentrations of dopants (Zn, Cd or Mn). The intersection of plotted lines at concentration equal zero represents austenite-martensite total energy difference for stoichiometric Ni_2MnGa and is taken as the reference value. The first assumption is that all the ascending lines represent alloys with higher values of martensite transformation temperature than T_M of nonmodified alloy. The second assumption is that a steepness lines tells us how rapid this increase should be. In particular, both lines representing Cd or Zn in the Ga-sublattice as well as line corresponding to the off-stoichiometric alloys ascend and these types of doping should increase T_M. These predictions are in a very good agreement with the experimental data. It was found out that the substitution of Ga with Zn increased the austenite transformation temperature by 79 K and 114 K for zinc concentrations of 2at% and 3 at%, respectively [31]. Also experiments for off-stoichiometric alloys support theoretical data presented in this work, namely the increase of the austenite transformation temperature by 135 K and 158 K for alloys with 3.9 at% and 4.8 at% of Mn at Ga sites [26]. In Figure 6.4 are plotted also results for doping with Cu adopted from [35]. Both Cu → Ga and

Cu → Mn energy difference dependencies ascend, predicting the increase in T_M for both types of doping. This was confirmed by experimental data, as substitution of 2.5 at% and 5 at% of Cu for Ga leads to the T_M rise by roughly 120 K and 320 K, respectively. Doping of Cu instead of Mn resulted in the T_M rise by roughly 50 K and 70 K, respectively [30]. The steepness of the Cu → Ga doping line is higher than of the Zn → Ga line and the rate of T_M growth is bigger. The same can be said about Zn → Ga and Cu → Mn dopings. However, the Mn → Ga doping is the steepest, but its experimentally observed effect on T_M is comparable to that of Zn substitution in the Ga sublattice. Introduced experimental data confirm the first above assumption, but the second one is disputed by the Mn → Ga doping. This is probably caused by the antiferromagnetic nature of $Ni_2Mn_{1+x}Ga_{1-x}$ alloys. Otherwise, the second assumption was confirmed for ferromagnetic alloys studied in this work.

On the other hand, doping the Mn-sublattice with either of Zn or Cd results in descending lines, predicting a decrease in T_M as a result of this type of modification.

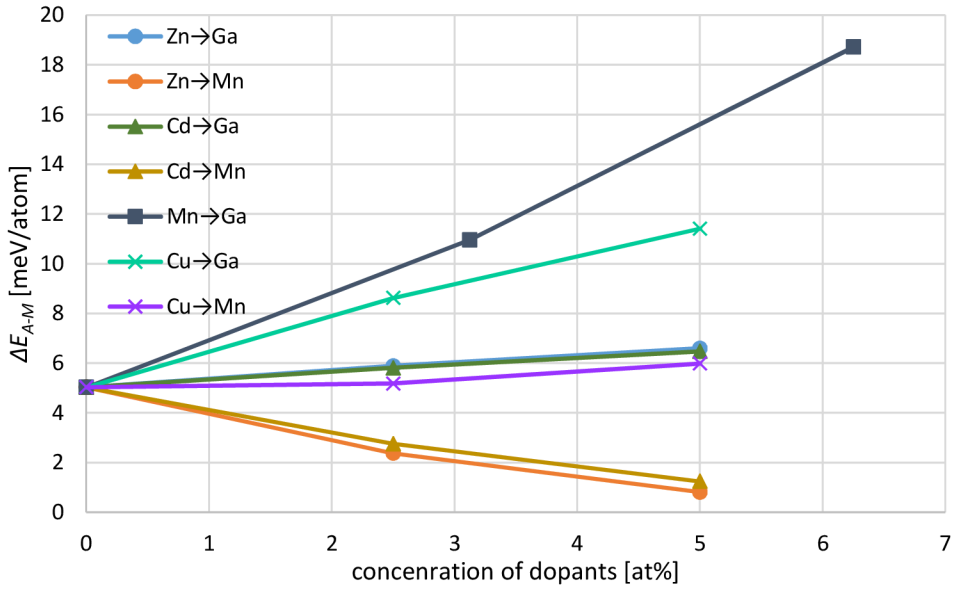

Figure 6.4 Energy differences between austenite and non-modulated martensite in FM state for alloys with various concentration of dopant in corresponding sublattice.

When considering the *e/a* rule, the number of valence electrons of Mn, Ni, Ga is set to be 7, 10 and 3. Doping elements Zn and Cd have each of 12 valence electrons. The *e/a* ratio of Ni_2MnGa, equal to 7.5, is then increased by Zn or Cd doping at any site. Referring to the *e/a* rule, this should indicate an increase in T_M, but trends are different for alloys with modifications in Mn sublattice. Findings in this and several previous works [5,33,61,62] disclaim a validity of the *e/a* rule for predicting trends of T_M changes for doped Ni-Mn-Ga systems. The energy differences between austenite and martensite for studied systems as well as the corresponding *e/a* ratios are listed in the Table 3.

Table 3 Energy differences between ferromagnetic and paramagnetic states in meV/atom, crucial for T_M and T_C predictions, and heats of formation for some alloys. Martensite is denoted by letter M, austenite is denoted by letter A.

Alloy	$\Delta E_{A\text{-}M}$	MARTENZITE $\Delta E_{PM\text{-}FM}$	AUSTENITE $\Delta E_{PM\text{-}FM}$	*e/a*
$Ni_{50}Mn_{25}Ga_{25}$	5.0341	29.8101	23.8236	7.50
$Ni_{50}Mn_{25}Ga_{20}Zn_5$	6.5988	28.5856	24.1909	7.95
$Ni_{50}Mn_{20}Ga_{25}Zn_5$	0.8163	19.0480	15.1431	7.75
$Ni_{50}Mn_{25}Ga_{20}Cd_5$	6.4789	27.4861	23.0889	7.95
$Ni_{50}Mn_{20}Ga_{25}Cd_5$	1.2446	18.7687	14.9799	7.75
$Ni_{50}Mn_{31.25}Ga_{18.75}$	18.7214	37.8374	23.8644	7.75

6.5 Prediction of Curie temperature

In order to predict behaviour of the Curie temperature, calculations of the tetragonal deformation paths were performed in paramagnetic states employing the DLM approximation. Predictions of T_C are based on the study of energy differences between FM and PM states. This method, as well as the method used for predicting T_M, are not able to give us accurate value of the transformation temperature but we can presume its trends in comparison with stoichiometric Ni_2MnGa. If the energy difference between PM and FM states for doped structure lowers in comparison with the undoped alloy, T_C will likely decrease and vice versa. Since we cannot determine the martensitic transformation temperature of studied alloys, we predict a change in Curie temperature of both austenite and martensite FM-PM transformations. However, in real systems, only one of mentioned magnetic transformations takes place depending on T_M (if $T_M > T_C$ then the real Curie temperature occurs in martensite and is denoted as T_C^M, if $T_M < T_C$ then the real Curie temperature occurs in austenite and is denoted as T_C^A). Computed tetragonal deformation paths for both FM and PM states are shown in Figure 6.5, both magnetic states are related to the FM austenite energy of given composition.

There were assumed two magnetic transformations in this work – FM austenite to PM austenite and FM martensite to PM martensite. If we will consider the unmodified Ni_2MnGa alloy (represented by red colour), the FM energy profile defines martensite as a ground state structure of the FM state. The PM state energy profile demonstrates energy minimum for the PM austenite solely, indicating that the PM martensite is unlikely the structure of PM state [54]. The conclusion resulting from these information is that pure Ni_2MnGa undergoes transformations in following order: FM martensite (the ground state structure) → FM austenite → PM austenite. Such a prediction made just from knowing the shape of tetragonal deformation paths is correlating with an experimental data, as T_M was measured to be at around 200 K and T_C^A at around 370 K. [63-65]

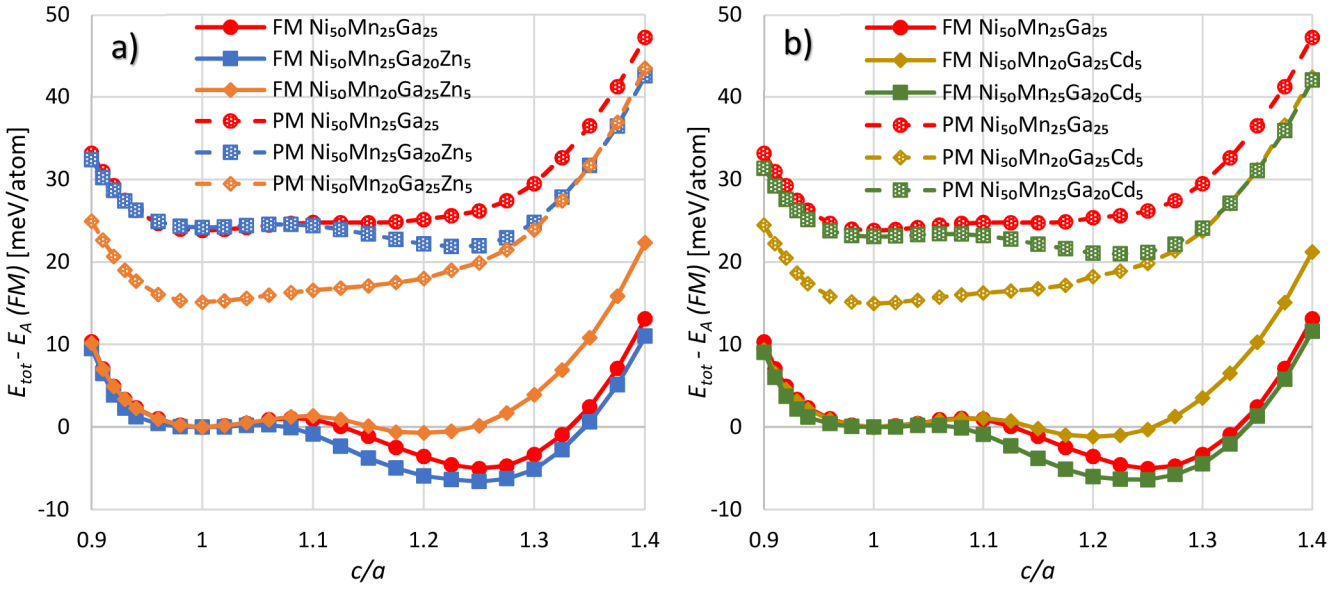

Figure 6.5 Tetragonal deformation paths for FM and PM states for 5 at% of Cd dopant a), and tetragonal deformation paths for FM and PM states for 5 at% of Zn dopant b).

As follows from Figure 6.5, Zn and Cd have almost the same effects in both magnetic states. From analysis of deformation paths for doping to Mn sublattice in PM states, it is obvious that only stable paramagnetic structure is austenite. The data presented in Figure 6.7 show that energy differences of FM and PM austenites (for Mn-sublattice doping) are smaller for both types of doping than in unmodified alloy. This fact can be linked to the decrease in Curie temperature. Effects of Zn and Cd are again identical. If we look at the FM states of the Mn-sublattice doping (orange and yellow energy profiles in figure 6.5) and Figure 6.4, we can forecast a decrease of T_M. It is probable that at higher concentrations of Zn or Cd in this sublattice, the FM austenite would become the ground state structure. Thus, substitution of Mn atoms should result in lowering of both T_M and T_C at studied concentrations and a likely transformation scenario is as follows: FM martensite → FM austenite → PM austenite.

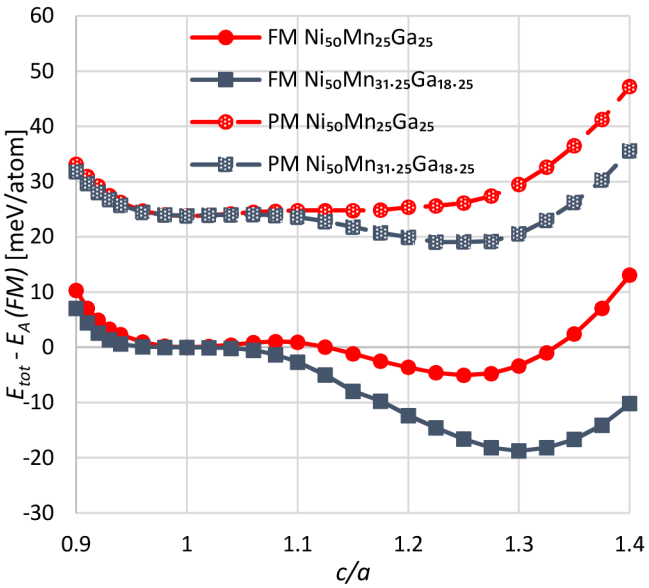

Figure 6.6 Tetragonal deformation paths for FM and PM states for 6.25 at% of Mn substituting Ga.

Considering the substitution of Ga atoms by Cd or Zn, Figure 6.7 shows descending dependences for transformation in martensite and almost constant dependences for

transformation in austenite. From this we can assume that a positive effect on T_C has neither of dopants considered in this work in Ga-sublattice. It is visible from figure 6.5 that there are two energy minima present in the PM states. It means that both austenite and martensite may be possibly found in PM state, and therefore it is difficult to specify the appropriate order transformations. Doping the Ga sites by Zn or Cd increases T_M and decreases Curie temperature.

From analysis of Figure 6.6, we can state that the Mn → Ga doping in the PM state should have similar effect as Zn or Cd doping in Ga sites (stabilization of PM martensite). The plot in Figure 6.7 confirms the above assumption for the FM austenite → PM austenite transformation, however, if the transformation occurs in martensite, it should have a positive effect on T_C^M. From experimental data we know that $T_M < T_C^A$ (Curie temperature for 3.9 at% and 4.8 at% in this order equals to 374 K and 370 K [26]) and hence the line carrying information about Cutie temperature is the line for austenite. Prediction for magnetic transformation in martensite is much more optimistic which should indicate an increase in Curie temperature. Experimental data proved further decrease of T_C for higher concentrations of Mn, making this prediction inaccurate. [26]. This disagreement is probably caused by the usage of DLM approximation for modelling of antiferromagnetic off-stoichiometric alloys with excess of Mn at expose of Ga.

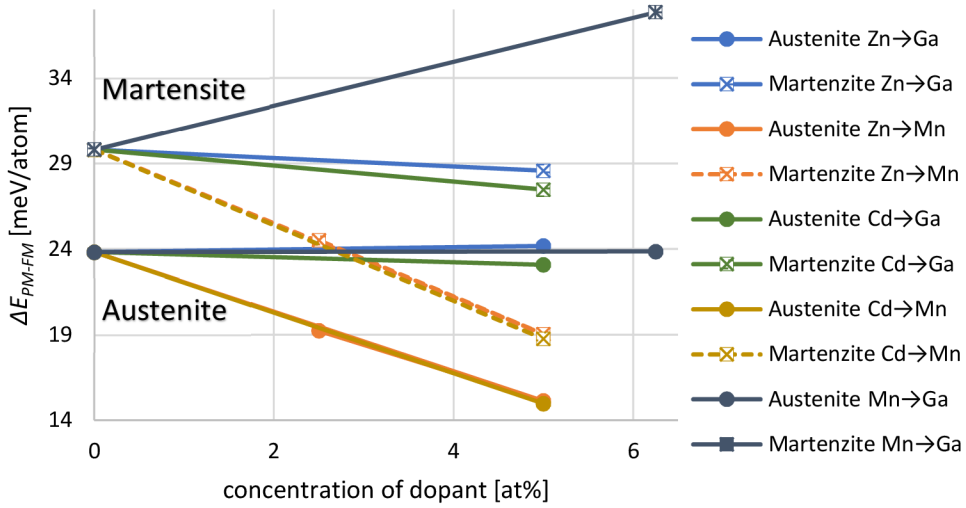

Figure 6.7 Energy differences between FM and PM structures of Zn and Cd doped alloys with 5 at% of dopants at every atom site. Magnetic transitions in martensite are symbolized by squares, transitions in austenite are represented by dots. The dashed lines represent unlikely transformations.

6.6 Electronic structure

The effect of doping on electronic structure of Ni-Mn-Ga alloys was also studied in order to explain observed relations and to examine the local stability of austenite. In Appendix, minority and majority DOS channels are plotted for austenite (a - d) and martensite (e – i). Majority DOS channels do not play such important role in stability of Ni-Mn-Ga alloys as minority channels and therefore the former are not commented in this work. By analysis of minority spin channel of density of states (DOS), we can address stability of austenite to formation of a pseudogap. The pseudogap in pure Ni_2MnGa austenite is located about 0.65 eV below E_f (the Fermi level). The creation of a pseudogap can be defined as a result of hybridization or interaction of Fermi surface and Brillouin zone [28], resulting in creation of an Ni-Ni antibonding peak near the Fermi energy, which is related to a Jahn-Teller instability. In this model, the lattice distortion breaks the degeneracy of *d* bands near E_f and thus cause a redistribution of electrons with

resulting reduction of energy [66]. A shallow and narrow pseudogap indicates weaker covalent bonding [67].

The antibonding peak located approximately 0.2 eV below E_f is responsible for instability of austenite, since a high density of states near E_f increase total energy of the cubic phase and makes it instable. Similarly, the tetragonal distortion is accompanied with motion of the antibonding peak over the Fermi level which cause existence of energy barrier in the tetragonal deformation path [35]. In Figure 6.8, there are compared total densities of states in austenite phase for undoped Ni_2MnGa and doped alloys. The substitution of Ga atoms by Zn or Cd have the same effect on electronic structure around E_f, but differs for states with lower energy. This substitution moves both the pseudogap and the antibonding peak closer to E_f and increases density of states on the Fermi energy comparing to the undoped alloy. This is also responsible for destabilization of the cubic austenite. On the contrary, substitution of Mn atoms by Zn or Cd fills the pseudogap and lowers the antibonding peak. This behaviour is linked to the stabilization of austenite and consequently to the decrease of T_M.

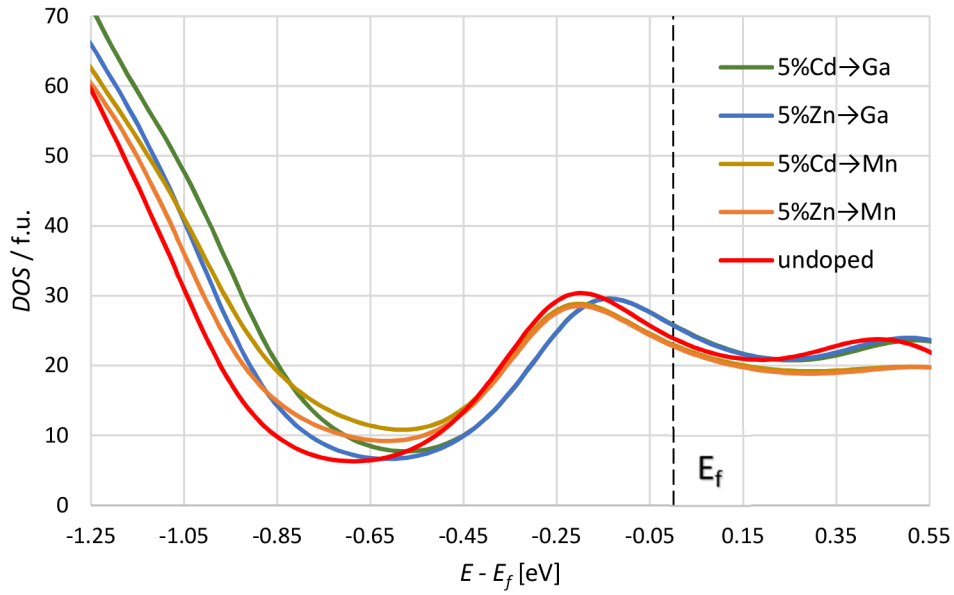

Figure 6.8 Comparison of total DOS majority spin channels for austenite phases of undoped and doped alloys.

The DOS plots for minority spin channel for studied alloys in martensitic phase are plotted in Figure 6.9. The stability of martensite phase in the undoped alloy is pronounced by shift of the antibonding peak over the Fermi level. Doping in Ga sublattice results in a shift of both pseudogap and antibonding peak towards higher energies. The pseudogap in DOS of the undoped alloy is slightly deeper. The minimization of density of states on the Fermi level is not present and hence a positive effect of doping in Ga sublattice is caused by destabilization of the austenite phase. However, doping in Mn sublattice affects neither pseudogap position nor its depth. A shift of the antibonding peak over E_f is not as strong as for the Ga substitution and not even as in the Ni_2MnGa alloy, hence stability of martensite is less resounding. Effects of Zn and Cd are again almost the same. The results of DOS calculations correspond to and support outcomes from analysis of tetragonal deformation paths.

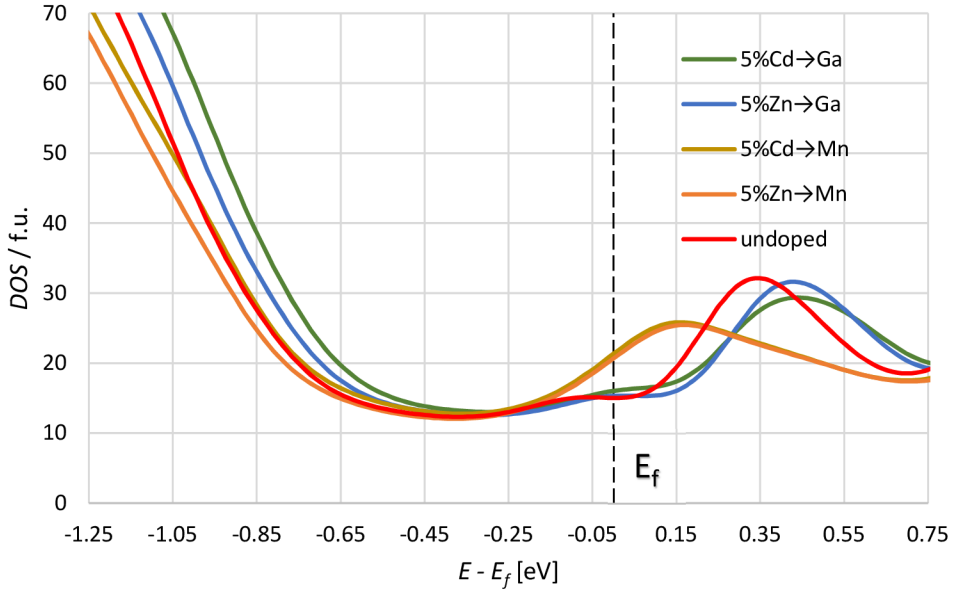

Figure 6.9 Comparison of total DOS majority spin channels of undoped and doped alloys in martensite phase.

Conclusion

This work dealt with theoretical study of Ni-Mn-Ga magnetic memory systems using *ab initio* calculations. Goal of this work was primarily focused on the prediction of effects of doping with Zn and Cd on transformation temperatures. In addition, the investigation of an off-stoichiometric $Ni_2Mn_{1+x}Ga_{1-x}$ alloy was performed. Sought properties were thermodynamic stability of alloys, martensite transformation temperature T_M, Curie temperature T_C and electronic structure.

All obtained results for Zn and Cd dopings show significant similarities when comparing substitutions in identical sublattices. Tetragonal deformation paths and energy differences in both ferromagnetic and paramagnetic states are identical for Zn and Cd substitutions. Since both elements are from the same group of the periodic table, an assumption was made that elements from one group have the same effects on Ni-Mn-Ga system in general.

The calculation of the heat of formation proved all studied alloys to be thermodynamically stable at temperature 0 K. Development of T_M can be predicted based on the analysis of the total energy along the tetragonal deformation path in ferromagnetic state. Substitutions of Zn or Cd for Ga atoms resulted in an increase in T_M. On the other hand, doping of both Zn and Cd for Mn influenced the system in a negative way and resulted in decrease in T_M. The information obtained from the study of the total energy development along the tetragonal deformation path were interpreted by analysis of DOS for Zn and Cd doped alloys. Doping in Ga sublattice was found to destabilizes austenite and to move the Ni-Ni antibonding peak above the Fermi level in matensite. These effects are responsible for increase in T_M. However, doping for Mn stabilized austenite and did not push the antibonding peak over the Fermi level completely.

The studied change in stoichiometry resulted markedly in the steepest growth of austenite-martensite energy difference with increasing concentration of Mn. This behaviour should correspond to the most significant increase in T_M, yet experimental data show that effect of doping with Zn in Ga sublattice is similar to that of the growth in Mn content. The observed behaviour and the deviation from the rule may be caused by antiferromagnetic nature of the off-stoichiometric alloy.

Predictions of Curie temperature were based on comparison of the total energies along tetragonal deformation paths in paramagnetic and ferromagnetic states. The results indicate a negative (decrease) or negligible effect on T_C for all types of doping apart from the magnetic transformation in martensite phase in the off-stoichiometric alloy. Thus, the growth of T_C could be expected with increasing concentration of Mn, which is in contradiction with experimental data probably also due to antiferromagnetic nature of this alloy. Both Zn and Cd cause a decrease in tetragonality in both sublattices, on the other hand, the tetragonality in the off-stoichiometric alloy rises.

The predictions done for the Zn doping in the Ga sublattice are supported by experimental results reported in available literature. This agreement validates also predictions of development of T_M made in his work as well as the method based on the comparison of energy differences between austenite and martensite.

Bibliography

[1] D. A. PORTER, K. E EASTERLING. and M. Y. SHERIF. *Phase Transformations in Metals and Alloys*. 3rd ed. London: CRC Press, 2009. ISBN 0412450305.

[2] J. ROGAL, K. REUTER and M. SCHEFFLER. *CO oxidation at Pd (100): A first-principles constrained thermodynamics study*. Physical Review B, 2007, **75**, p. 205433. DOI: 10.1103/PhysRevB.75.205433.

[3] J. N. LALENA and D. A. CLEARY. *Principles of Inorganic Materials Design*. 2nd ed. Hoboken, N.Y.: John Wiley, 2010. ISBN 978-0-470-40403-4.

[4] H. LEDBETTER, A. SAXENA, A. MIGLIORI. *Diffusionless Transformations, in:* G. F. BASSANI, G. L. LIEDL and P. WYDER (eds.), *Encyclopedia of condensed matter physic*. Oxford: Elsevier Science, 2005. pp. 429-437. ISBN: 978-0-12-369401-0.

[5] C.-M. LI, H.-B. LUO, Q.-M. HU, R. YANG, B. JOHANSSON and L. VITOS. *Site preference and elastic properties of Fe-, Co-, and Cu-doped Ni_2MnGa shape memory alloys from first principles*. Physical Review B, 2011, **84**, p. 024206. DOI: 10.1103/PhysRevB.84.024206.

[6] Y. MNYUKH. *On the Phase Transitions That Cannot Materialize*. American Journal of Condensed Matter Physics, 2013, **4**, pp. 1-12. DOI: 10.5923/j.ajcmp.20140401.01.

[7] S. YANG, X.-B.. REN and X.-P. SONG. *Evidence for first-order nature of the ferromagnetic transition in Ni, Fe, Co, and $CoFe_2O_4$*. Physical Review B, 2008, **78**, p. 174427. DOI: 10.1103/PhysRevB.78.174427.

[8] Y. MNYUKH. *Fundamentals of solid-state phase transitions, ferromagnetism and ferroelectricity.* 2nd. ed. Farfield: 1st Books, 2009. ISBN 978-0-615-33972-6.

[9] J. PONS, V. A. CHERNENKO, R. SANTAMARTA, and E. CESARI. *Crystal structure of martensitic phases in Ni–Mn–Ga shape memory alloys*. Acta Materialia, 2000, **48**, pp. 3027-3038. DOI: 10.1016/S1359-6454(00)00130-0.

[10] H. K. D. H. BHADESHIA. *Martensitic transformation, in:* K. BUSCHOW, R. W. CAHN, M. C. FLEMINGS, B. LISCHER, E. J. KRAMER and S. MAHAJAN (eds.), *Encyclopedia of Materials Science: Science and Technology*. Pergamon Press, Elsevier Science, 2001. pp. 5203-5206. ISBN 0-08-0431526.

[11] V. VODÁREK. *Phase transformations: didactic text.* Ostrava: VŠB – Technická univerzita Ostrava, 2013. ISBN 978-80-248-3376-7.

[12] A. DANNENBERG. *Ab initio and Monte Carlo investigations of structural, electronic and magnetic properties of new ferromagnetic Heusler alloys with high Curie temperatures.* Duisburg, 2011. PhD thesis. University of Duisburg-Essen. Faculty of Physics.

[13] P. MÜLLNER and A. H. KING. *Deformation of hierarchically twinned martensite*. Acta Materialia, 2010, **58**, pp. 5242-5261. DOI: 10.1016/j.actamat.2010.05.048.

[14] J. M. D. COEY. *Magnetism and magnetic materials*. New York: Cambridge University Press, 2010. ISBN 978-0-521-81614-4.

[15] C. KITTEL. *Introduction to solid state physics*. 6 ed. New York: John Wiley, 1986. ISBN 0-471-87474-4.

[16] I. A. ABRIKOSOV, A. V. PONOMAREVA, P. STENETEG, S. A. BARANNIKOVA and B. ALLING. *Recent progress in simulations of the paramagnetic state of magnetic materials*. Current Opinion in Solid State & Materials Science, 2016, **20**, pp. 85-106. DOI: 10.1016/j.cossms.2015.07.003.

[17] O. HECZKO, N. SCHEERBAUM AND O. GUTFLEISCH. *Magnetic shape memory phenomena,in:*J. LIU, E. FULLERTON, E. GUTFLEISCH and D. SELLMYER (eds.), *Nanoscale magnetic materials and applications*. New York, N.Y.: Springer Science & Business Media, 2009. pp. 339-439. ISBN 978-3-387-85598-1.

[18] F. HEUSLER and E. TAKE. *The nature of the Heusler alloys*. Transactions of the Faraday Society, 1912, **8**, pp. 169-184. DOI: 10.1039/TF9120800169.

[19] I. GALANAKIS. *Theory of Heusler and Full-Heusler Compounds, in:* C. FELSER, A. HIROHATA (eds.), *Heusler Alloys*. Springer Series in Materials Science, 2016, **222**. pp. 3-36. DOI: 10.1007/978-3-319-21449-8_1.

[20] I. GALANAKIS, Ph. MAVROPOULOS and P. H. DEDERICHS. *Electronic structure and Slater-Pauling behaviour in half-metallic Heusler alloys calculated from first principles*. Journal of Physics D: Applied Physics, 2006, **39**, pp. 765-775. DOI: 10.1088/0022-3727/39/5/S01.

[21] P. J. WEBSTER, K. R. A. ZIEBECK, S. L. TOWN and M. S. PEAK. *Magnetic order and phase transformation in Ni_2MnGa*. Philosophical Magazine Part B, 1984, **49**, pp. 295-310. DOI: 10.1080/13642817408246515.

[22] M. ZELENÝ, L. STRAKA, A. SOZINOV and O. HECZKO. *Ab initio prediction of stable nanotwin double layers and 4O structure in Ni_2MnGa*. Physical Review B, 2016, **94**, p. 224108. DOI: 10.1103/PhysRevB.94.224108.

[23] J. KÜBLER, A. R. WILLIAM, C. B. SOMMERS. *Formation and coupling of magnetic moments in Heusler alloys*. Physical Review B, 1983, **28**, pp. 1745-1755. DOI: 10.1103/PhysRevB.28.1745.

[24] First-Ever Clarification of Mechanism of Shape Memory Effect Driven by Magnetic Field - Breakthrough towards Practical Use of High-Output Actuators (Press Release). In: spring8.or.jp . Kouto, Sayo-cho, Sayo-gun, Hyogo: Spring 8, 27.04.2010. Accessible from: http://www.spring8.or.jp/en/news_publications/press_release/2010/100427/

[25] V.A. CHERNENKO, *Compositional instability of β-phase in Ni-Mn-Ga alloys*. Scripta Materialia, 1999, **42**, pp. 523-527. DOI: 10.1016/S1359-6462(98)00494-1.

[26] N. LANSKA, O. SÖDERBERG, A. SOZINOV, Y. GE, K. ULLAKKO and V. K. LINDROOS. *Composition and temperature dependence of the crystal structure of Ni–Mn–Ga alloys*. Journal of Applied Physics, 2004, **95**, pp. 8074-8078. DOI: 10.1063/1.1748860.

[27] P. ENTEL, V. D. BUCHELNIKOV, V. V. KHOVAILO, A. T. ZAYAK, W. A. ADEAGBO, M. E. GRUNER, H. C. HERPER and E. F. WASSERMANN. *Modelling the phase diagram of magnetic shape memory Heusler alloys*. Journal of Physics D: Applied Physics, 2006, **39**, pp. 865-889. DOI: 10.1088/0022-3727/39/5/S13.

[28] U. MIZUTANI. *Hume-Rothery Rules for Structurally complex Alloy Phases*. Boca Raton, FL: Taylor & Francis Group, 2011. ISBN: 978-1-4200-9059-8.

[29] A. SOZINOV, N. LANSKA, A. SOROKA and W. ZOU. *12% magnetic field-induced strain in Ni-Mn-Ga-based non-modulated martensite.* Applied Physics Letters, 2013, **102**, p. 021902. DOI: 10.1063/1.4775677.

[30] T. KANOMATA, K. ENDO, N. KUDO, et al. *Magnetic moment of cu-modified Ni_2MnGa magnetic shape memory alloys*. Metals, 2013, **3**, pp. 114-122. DOI: 10.3390/met3010114.

[31] L. S. BARTON, R. T. LAZOTT and E. R. MARSTEN. *Magnetic properties of full Heusler alloys $Ni_2MnGa_{1-x}Z_x$ with Z = Sn or Zn*. Journal of Applied Physics, 2014, **115**, p. 17A908. DOI: 10.1063/1.4861217.

[32] A. PLANES, L. MAÑOSA, M. ACET. *Magnetocaloric effect and its relation to shape memory properties in ferromagnetic Heusler alloys.* Journal of Physics: Condensed Matter, 2009, **21**, p. 233201. DOI: 10.1088/0953-8984/21/23/233201.

[33] D. KIKUCHI, T. KANOMATA, Y. YAMAGUCHI, H. NISHIHARA, K. KOYAMA and K. WATANABE. *Magnetic properties of ferromagnetic shape memory alloys $Ni_2Mn_{1-x}Fe_xGa$*. Journal of Alloys and Compounds. 2004, **383**, pp. 184-188. DOI: 10.1016/j.jallcom.2004.04.053.

[34] L. CHEN, Y. LI, J. SHANG and H. XU. *First principles calculations on martensitic transformation and phase instability of Ni–Mn–Ga high temperature shape memory alloys.* Applied Physics Letters, 2006, **89**, p. 231921. DOI: 10.1063/1.2402891.

[35] M. ZELENÝ, A. SOZINOV, L. STRAKA, T. BJÖRKMAN and R. M. NIEMINEN. *First-principles study of Co- and Cu-doped Ni_2MnGa along the tetragonal deformation path*. Physical Review B, 2014, **89**. DOI: 10.1103/PhysRevB.89.184103.

[36] L. VITOS. *The exact muffin-tin orbitals method and applications*. Budapest, 2008. PhD Thesis. Hungarian Academy of Sciences. Research institute for Solid State Physics and Optics.

[37] M. SPRINGBORG. *Methods of Electronic-Structure Calculations: From Molecules to Solids.* Chichester: John Wiley: 2000. ISBN: 978-0-471-97975-3.

[38] P. HOHENBERG, W. KOHN. *Inhomogeneous electron gas.* Physical Review, 1964, **136**, pp. B864-B871. DOI: 10.1103/PhysRev.136.B864.

[39] W. KOHN, L. J. SHAM. *Self-consistent equations including exchange and correlation effects.* Physical Review, 1965, **140**, pp. A1133-A1138. DOI: 10.1103/PhysRev.140.A1133.

[40] K. CAPELLE. *A Bird's-Eye View of Density-Functional Theory*. Brazilian Journal of Physics, 2006, **36**, pp. 1318-1343. DOI: 10.1590/S0103-97332006000700035.

[41] O. K. ANDERSEN, O. JEPSEN, and G. KRIER. *Exact Muffin-Tin Orbital Theory, in:* V. KUMAR, O. K. ANDERSEN, and A. MOOKERJEE (eds.), *Lectures on Methods of Electronic Structure Calculations.*, Singapore: World Scientific, 1994, pp. 63–124. ISBN: 978-981-4583-27-5.

[42] L. SZUNYOGH, B. ÚJFALUSSY, P. WEINBERGER, J. KOLLÁR. *Self-consistent localized KKR scheme for surfaces and interfaces.* Physical Review B, 1994, **49**, p. 2721. DOI: 10.1103/PhysRevB.49.2721.

[43] P. SOVEN. *Coherent-potential model of substitutional disordered alloys.* Physical Review, 1967, **156**, pp. 809-813. DOI: 10.1103/PhysRev.156.809.

[44] M. ZELENÝ and I. DLOUHÝ. *Different Ab Initio Approaches for Doping Descriptions: Tetragonal Deformation of Ni-Mn-Ga Alloys*. Solid State Phenomena, 2017, **258**, pp. 37-40. DOI: 10.4028/www.scientific.net/SSP.258.37.

[45] B. L. GYOFFY, A. J. PINDOR, J. STAUNTON, G. M. STOCKS and H. WINTER. *A first-principles theory of ferromagnetic phase transitions in metals.* Journal of Physics F: Metal Physics, 1985, **15**, pp. 1137-1386. DOI: 10.1088/0305-4608/15/6/018.

[46] L. VITOS. *Computational Quantum Mechanics for Materials Engineers: The EMTO Method and Applications*. London: Springer London, 2007. ISBN 9781846289507.

[47] M. DEHGHANI. *Development of Advanced Computational Techniques for Alloys in Complex Atomic and Magnetic Configurational States*. Leoben, 2017. PhD thesis. Materials Center Leoben Forschung GmbH. Supervisor: Peter Puschnig and Andrei Ruban.

[48] EMTO. Manual. c2018. Accessible from: http://emto.gitlab.io/manual/manual.html

[49] J. P. PERDEW, K. BURKE and M. ERNZERHOF. *Generalized Gradient Approximation Made Simple*. Physical Review Letters. 1996, **77**, pp. 3865-3868. DOI: 10.1103/PhysRevLett.77.3865.

[50] P. A. KORZHAVYI, A. V. RUBAN, I. A. ABRIKOSOV, H. L. SKRIVER. *Madelung energy for random metallic alloys in the coherent potential approximation.* Physical Review B, 1995, **51**, pp. 5773-5780. DOI: 10.1103/PhysRevB.51.5773.

[51] A.V. RUBAN, H. L. SKRIVER. *Screened Coulomb interactions in metallic alloys. I. Universal screening in the atomic-sphere approximation.* Physical Review B, 2002, **66**, p. 024201. DOI: 10.1103/PhysRevB.66.024201.

[52] C.-M- LI, Q.-M. HU, R. YANG, B. JOHANSSON and L. VITOS. *Interplay between temperature and composition effects on the martensitic transformation in $Ni_{2+x}Mn_{1-x}Ga$ alloys*. Applied Physics Letters, 2011, **98**, p. 261903. DOI: 10.1063/1.3603935.

[53] Q.-M. HU, H.-B. LUO, C.-M. LI, L. VITOS, and R. YANG. *Composition dependent elastic modulus and phase stability of Ni2MnGa based ferromagnetic shape memory alloys.* Science China Technological Sciences, 2012, **55**, pp. 295-305. DOI: 10.1007/s11431-011-4670-z.

[54] M. ZELENÝ, A. SOZINOV, T. BJÖRKMAN, L. STRAKA, O. HECZKO and R. M. NIEMINEN. *Effect of Magnetic Ordering on the Stability of Ni–Mn–Ga(–Co–Cu) Alloys Along the Tetragonal Deformation Path*. IEEE Transactions on Magnetics, 2017, **53**, pp. 1-6. DOI: 10.1109/TMAG.2017.2707527.

[55] J. B. STAUNTON. *The electronic structure of magnetic transition metallic materials.* Reports on Progress in Physics, 1994, **54**, pp. 1289-1344. DOI: 10.1088/0034-4885/57/12/002.

[56] J. ENKOVAARA, O. HECZKO, A. AYUELA, and R. M. NIEMINEN. *Coexistence of ferromagnetic and antiferromagnetic order in Mn-doped Ni_2MnGa.* Physical Review B 2003, **67**, p. 212405. DOI: 10.1103/PhysRevB.67.212405.

[57] S. ÖZDEMIR KART, M. ULUDOĞAN, I. KARAMAN and T. ÇAĞIN. *DFT studies on structure, mechanics and phase behavior of magnetic shape memory alloys: Ni_2MnGa*. Physica status solidi (a). 2008, **205**, pp. 1026-1035. DOI: 10.1002/pssa.200776453.

[58] H.-B. LUO, Q.-M. HU, C.-M. LI, R. YANG, B. JOHANSSON and L. VITOS. *Phase stability of $Ni_2(Mn_{1-x}Fe_x)Ga$: A first-principles study*. Physical Review B, 2012, **86**, p. 024427. DOI: 10.1103/PhysRevB.86.024427.

[59] M. YIN, P. NASH, W. CHEN and S. CHEN. *Standard enthalpies of formation of selected Ni2YZ Heusler compounds*. Journal of Alloys and Compounds, 2016, **660**, pp. 258-265. DOI: 10.1016/j.jallcom.2015.11.126.

[60] M. ZELENÝ, L. STRAKA, A. SOZINOV, O. HECZKO. *Transformation Paths from Cubic to Low-Symmetry Structures in Heusler Ni_2MnGa Compound*. Scientific Reports, 2018, **8**, p. 7275. DOI: 10.1038/s41598-018-25598-z.

[61] D.E. SOTO-PARRA, X. MOYA, L. MAÑOSA, et al. *Fe and Co selective substitution in Ni_2MnGa: Effect of magnetism on relative phase stability*. Philosophical Magazine, 2010, **90**, pp. 2771-2792. DOI: 10.1080/14786431003745393.

[62] Z. H. LIU, M. ZHANG, W. Q. WANG, et al. *Magnetic properties and martensitic transformation in quaternary Heusler alloy of NiMnFeGa*. Journal of Applied Physics, 2002, **92**, pp. 5006-5010. DOI: 10.1063/1.1511293.

[63] B. DUTTA, A. ÇAKIR, C. GIACOBBE, A. AL-ZUBI, T. HICKEL, M. ACET and J. NEUGEBAUER. *Ab initio Prediction of Martensitic and Intermartensitic Phase Boundaries in Ni-Mn-Ga*. Physical Review Letters. 2016, **116**, p. 025503. DOI: 10.1103/PhysRevLett.116.025503.

[64] V. DOBREA, M. LOZOVAN, M. CRAUS and V. SIMKIN. *Some physical properties of Ni_2MnGa Heusler shape memory alloys with substitutions*. Journal of Optoelectronics And Advanced Materials, 2010, **12**, pp. 854-857.

[65] Y. MA, S. AWAJI, K. WATANABE, M. MATSUMOTO and N. KOBAYASHI. *Investigation of phase transformations in Ni_2MnGa using high magnetic field low-temperature X-ray diffraction system*. Physica B, 2000, **284**, pp. 1333-1334. DOI: 10.1016/S0921-4526(99)02615-0.

[66] P. J. BROWN. *Direct observation of a band Jahn-Teller effect in the martensitic phase transition of Ni_2MnGa*. Journal of Physics: Condensed Matter. 1999, **11**, pp. 4715-4722. DOI: 10.1088/0953-8984/11/24/312.

[67] C.-M. LI, H.-B. LUO, Q.-M. HU, R. YANG, B. JOHANSSON and L. VITOS. *First-principles investigation of the composition dependent properties of $Ni_{2+x}Mn_{1-x}Ga$ shape-memory alloys*. Physical Review B, 2010, **82**, p. 024201. DOI: 10.1103/PhysRevB.82.024201.

List of abbreviations and symbols

Abbreviation	Meaning		
FCC	Face centred cubic lattice	**MSM**	Magnetic shape memory
BCT	Body centred tetragonal lattice	**DOS**	Density of states
NM	Non-modulated martensite	**DFT**	Density functional theory
10M	five-layered modulated martensite	**EMTO**	Exact Muffin-Tin Orbitals
14M	Seven-layered modulated martensite	**KKR**	Korringa-Kohn-Rostoker
4O	Four-layered modulated martensite	**CPA**	Coherent Potential Approximation
$L2_1$	Cubic full-Heusler lattice	**PBE**	Perdew-Burke-Ernzerhof
$C1_b$	Cubic semi-Heusler lattice	**PAW**	Projector augmented vawe
MIR	Magnetically induced reorientation	**FM**	Ferromagnetic state
MFIS	Magnetic field-induced strain	**PM**	Paramagnetic state

Symbol	Unit	Characterization
G	eV	Gibbs energy
E_{tot}	eV	Total energy
F	eV	Free energy
p	Pa	Pressure
V	m^3	volume
S	$JK^{-1}mol^{-1}$	entropy
U	eV	Internal energy
T	K	Temperature
H	eV	Enthalpy
ΔH_f	eV	Heat of formation
T_M	K	Martensitic transformation temperature
T_C	K	Curie temperature
$C´$	Pa	Tetragonal shear modulus
R_{ws}	Å	Wigner-Seitz radius
V_{0A}	$Å^3$	Equilibrium volume of austenitic primitive cell
ΔH_f^A	eV	Heat of formation of austenite
E_A	eV	Total energy of austenite
E_M	eV	Total energy of martensite
μ_{tot}	μ_B	Total magnetic moment per formula unit
$\Delta E_{A\text{-}M}$	eV	Total energy difference between austenite and martensite
$\Delta E_{PM\text{-}FM}$	eV	Total energy difference between PM and FM state
T_C^A	K	Curie temperature in austenite
T_C^M	K	Curie temperature in martensite
E_f	eV	Fermi level
c/a	-	Tetragonality
e/a	-	Valence electron density
$(c/a)_{NM}$	-	Tetragonality of NM martensite

Appendix

Minority (spin down) and majority (spin up) DOS channels. Plotted are total DOS per primitive cell and DOS per atom for every constituent atom. The total DOS is a sum of contributions from all constituents with respect to their content. Figures a) – e) represent austenite, f) – i) represent martensite.

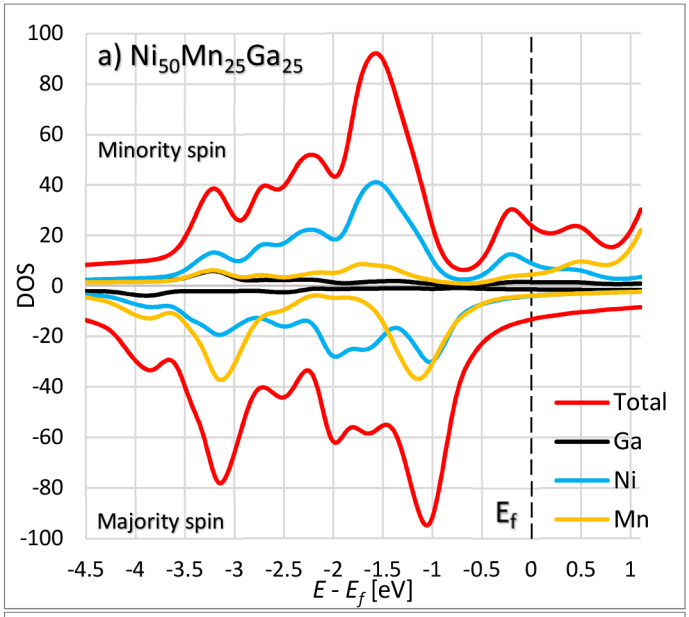

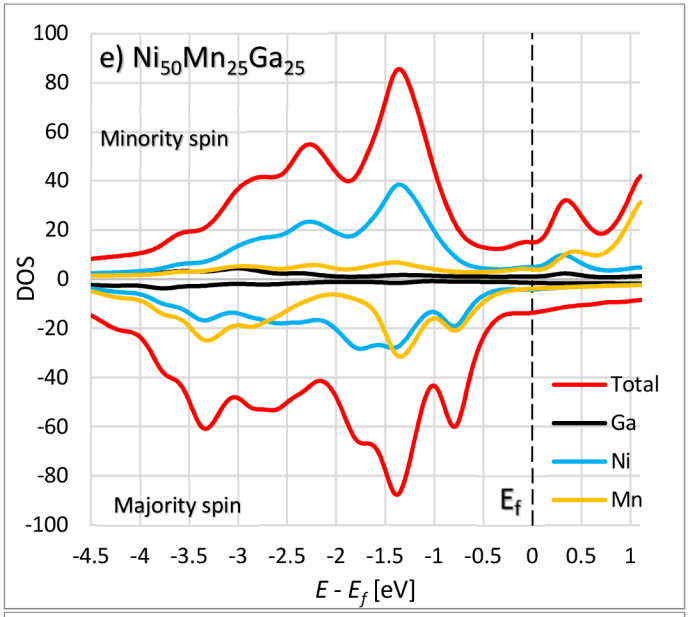

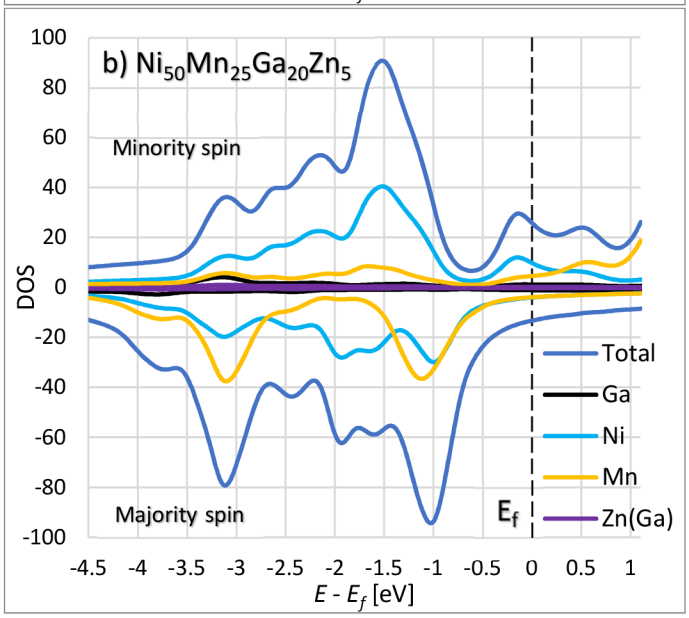

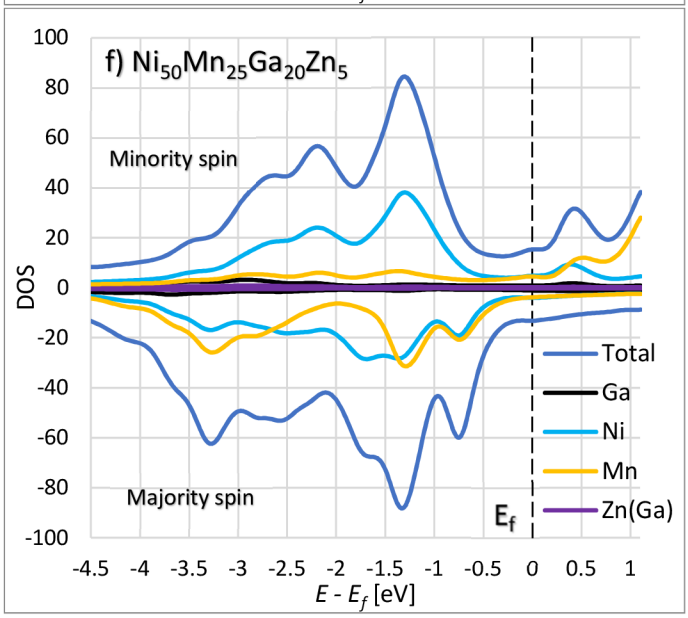

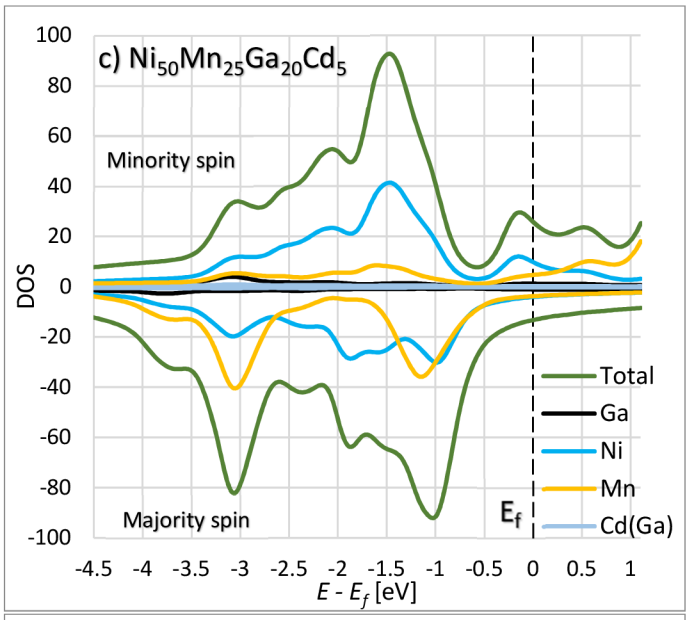
c) $Ni_{50}Mn_{25}Ga_{20}Cd_5$
Minority spin
Majority spin
DOS
$E - E_f$ [eV]
E_f
Total
Ga
Ni
Mn
Cd(Ga)

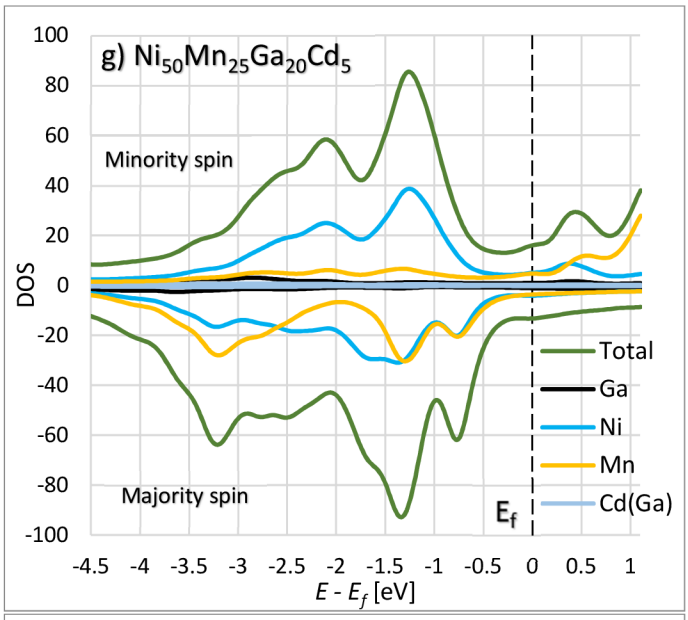
g) $Ni_{50}Mn_{25}Ga_{20}Cd_5$
Minority spin
Majority spin
DOS
$E - E_f$ [eV]
E_f
Total
Ga
Ni
Mn
Cd(Ga)

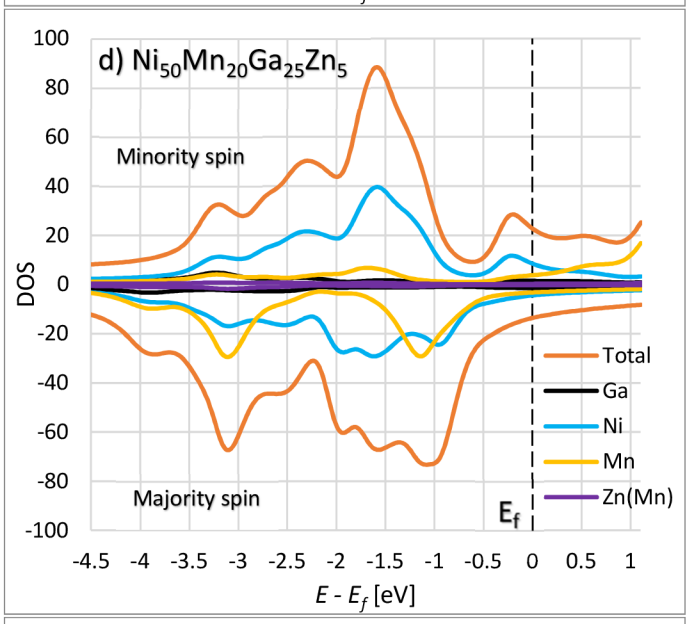
d) $Ni_{50}Mn_{20}Ga_{25}Zn_5$
Minority spin
Majority spin
DOS
$E - E_f$ [eV]
E_f
Total
Ga
Ni
Mn
Zn(Mn)

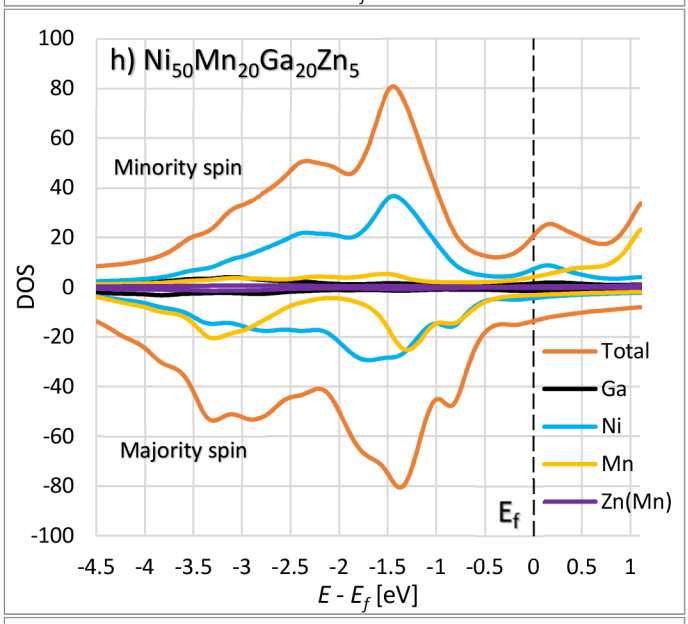
h) $Ni_{50}Mn_{20}Ga_{20}Zn_5$
Minority spin
Majority spin
DOS
$E - E_f$ [eV]
E_f
Total
Ga
Ni
Mn
Zn(Mn)

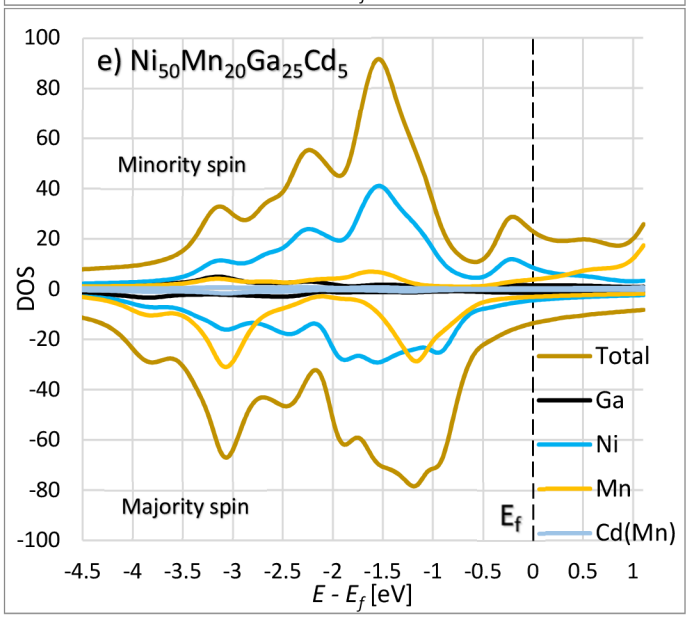
e) $Ni_{50}Mn_{20}Ga_{25}Cd_5$
Minority spin
Majority spin
DOS
$E - E_f$ [eV]
E_f
Total
Ga
Ni
Mn
Cd(Mn)

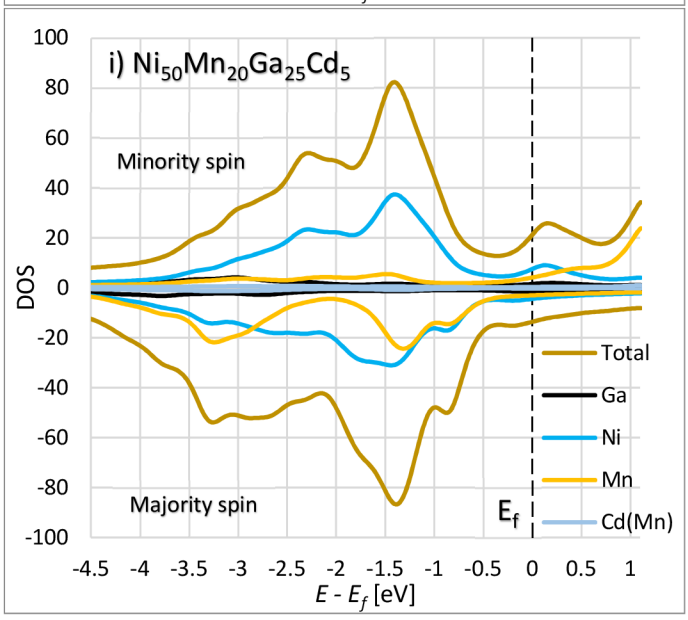
i) $Ni_{50}Mn_{20}Ga_{25}Cd_5$
Minority spin
Majority spin
DOS
$E - E_f$ [eV]
E_f
Total
Ga
Ni
Mn
Cd(Mn)